Discovery and Kinetic Profiling of 7-Aryl-1,2,4-triazolo[4,3-a]pyridines: Positive Allosteric Modulators of the Metabotropic Glutamate Receptor 2

Maarten L. J. Doornbos,[†] José María Cid,[‡] Jordi Haubrich,[†] Alexandro Nunes,[†] Jasper W. van de Sande,[†] Sophie C. Vermond,[†] Thea Mulder-Krieger,[†] Andrés A. Trabanco,[‡] Abdellah Ahnaou,[§] Wilhelmus H. Drinkenburg,[§] Hilde Lavreysen,[§] Laura H. Heitman,[†] Adriaan P. IJzerman,*,[†] and Gary Tresadern*,[‡]

[†]Division of Medicinal Chemistry, Leiden Academic Centre for Drug Research (LACDR), Leiden University, P.O. Box 9502, 2300RA Leiden, The Netherlands

[‡]Janssen Research and Development, Calle Jarama 75A, 45007, Toledo, Spain

[§]Janssen Research and Development, Turnhoutseweg 30, 2340 Beerse, Belgium

S Supporting Information

ABSTRACT: We report the synthesis and biological evaluation of a series of 7-aryl-1,2,4-triazolo[4,3-a]pyridines with mGlu$_2$ positive allosteric modulator (PAM) activity and affinity. Besides traditional in vitro parameters of potency and affinity, kinetic parameters k_{on}, k_{off} and residence time (RT) were determined. The PAMs showed various kinetic profiles; k_{on} values ranged over 2 orders of magnitude, whereas RT values were within a 10-fold range. Association rate constant k_{on} was linearly correlated to affinity. Evaluation of a short, medium, and long RT compound in a label-free assay indicated a correlation between RT and functional effect. The effects of long RT compound **9** on sleep−wake states indicated long RT was translated into sustained inhibition of rapid eye movement (REM) in vivo. These results show that affinity-only driven selection would have resulted in mGlu$_2$ PAMs with high values for k_{on} but not necessarily optimized RT, which is key to predicting optimal efficacy in vivo.
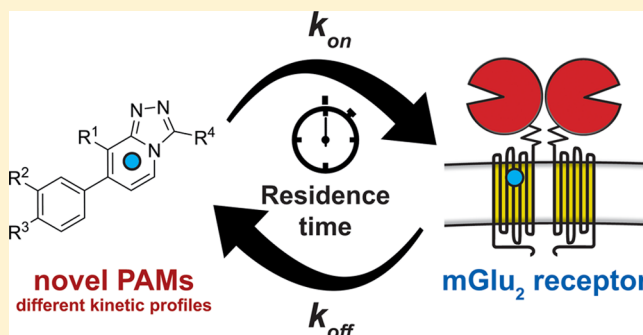
INTRODUCTION

Glutamate is an important neurotransmitter in the human central nervous system (CNS), where it modulates synaptic responses by activating ionotropic glutamate receptors (iGlu) and metabotropic glutamate receptors (mGlu).[1] The eight known mGlu receptors, which belong to the class C G-protein-coupled receptors (GPCRs), have been divided into three subclasses based on sequence homology, signaling pathway, and pharmacological profile: group I (mGlu$_{1,5}$), group II (mGlu$_{2,3}$), and group III (mGlu$_{4,6,7,8}$).[2] Structurally, class C GPCRs consist of a large extracellular orthosteric binding domain, the so-called Venus flytrap (VFT), a cysteine-rich domain connecting the VFT to the seven-transmembrane (7TM) domain.[2,3] Group II mGlu receptors are coupled to the G$\alpha_{i/o}$ protein and are generally expressed presynaptically in the periphery of the synapse where they inhibit the release of glutamate upon activation.[4] The activation of mGlu$_2$ receptors has been shown to be a potential strategy for the treatment of psychiatric diseases involving abnormal glutamatergic neurotransmission, such as schizophrenia and anxiety disorder.[5,6] Drug discovery efforts include the development of positive allosteric modulators (PAMs) for which

subtype selectivity can be more easily obtained as they bind within the less conserved 7TM domain and have little or no intrinsic activity on their own.[7,8] The mGlu$_2$ PAMs N-(4-(2-methoxyphenoxy)phenyl)-N-(2,2,2-trifluoroethylsulfonyl)-pyrid-3-ylmethylamine (**1**, LY487379),[9] biphenylindanone A (**2**, BINA),[10] N-(4-((2-(trifluoromethyl)-3-hydroxy-4-(isobutyryl)-phenoxy)methyl)benzyl)-1-methyl-1H-imidazole-4-carboxamide (**3**, THIIC, also known as LY2607540),[11] and 3-cyano-1-cyclopropylmethyl-4-(4-phenylpiperidin-1-yl)pyridine-2(1H)-one (**4**, JNJ-40068782)[12] (Figure 1) have been characterized both in vitro and in vivo. To date, two mGlu$_2$ PAMs have reached clinical trials. The development of 7-methyl-5-[3-(piperazin-1-ylmethyl)-1,2,4-oxadiazol-5-yl]-2-[[4-(trifluoromethoxy)-phenyl]methyl]-3H-isoindol-1-one (**5**, AZD8529) by AstraZeneca was discontinued after a phase 2 schizophrenia trial in which it did not show clinical efficacy when tested as monotherapy.[13,14] Compound **5** recently finished a phase II clinical trial to study smoking cessation in female smokers.[15]
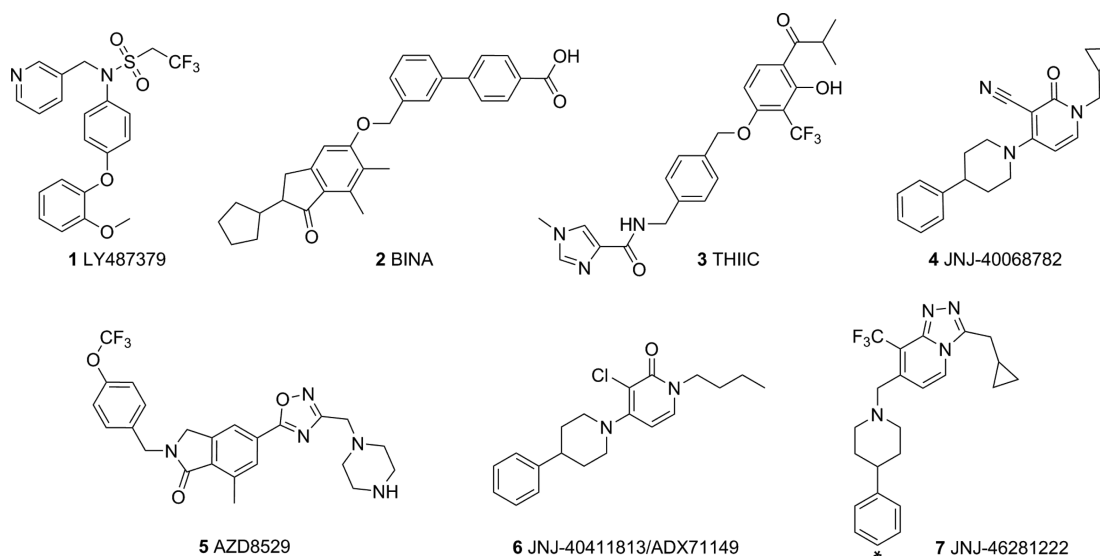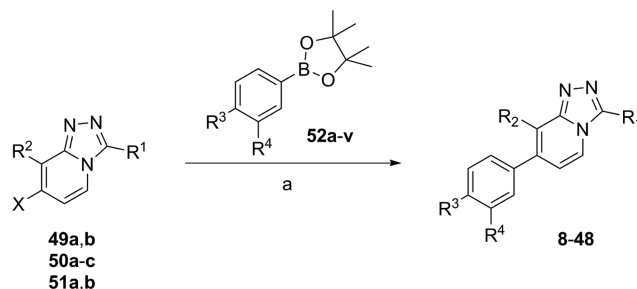
Figure 1. Structures of reference mGlu$_2$ PAMs. The position of the tritium label of [^{3}H]-7 is denoted by ∗.

Scheme 1. Synthesis of Final Compounds 8−48[a]

49a: R^1 = ^{c}propylmethyl; R^2 = CF$_3$; X = Cl
49b: R^1 = ethoxymethyl; R^2 = CF$_3$; X = Cl
50a: R^1 = ^{c}propylmethyl; R^2 = Cl; X = I
50b: R^1 = ethoxymethyl; R^2 = Cl; X = I
50c: R^1 = trifluoroethyl; R^2 = Cl; X = I
51a: R^1 = ^{c}propylmethyl; R^2 = Me; X = Cl
51b: R^1 = ^{c}propylmethyl; R^2 = ^{c}propyl; X = Cl

52a: R^3 = 2,6-dimethylpyridyl-3-oxy; R^4 = F
52b: R^3 = 2,6-dimethylpyridyl-3-oxy; R^4 = Cl
52c: R^3 = 2-methylpyridyl-4-oxy; R^4 = F
52d: R^3 = 2-ethylpyridyl-4-oxy; R^4 = F
52e: R^3 = 2,6-dimethylpyridyl-4-oxy; R^4 = F
52f: R^3 = 2-^{c}propylpyridyl-4-oxy; R^4 = F
52g: R^3 = ^{i}propylamino; R^4 = F
52h: R^3 = ^{i}propylamino; R^4 = Cl
52i: R^3 = ^{c}propylamino; R^4 = F
52j: R^3 = ^{c}propylamino; R^4 = Cl
52k: R^3 = 2-methoxypyridyl-5-methyloxy; R^4 = F
52l: R^3 = 2-methoxypyridyl-5-methyloxy; R^4 = H
52m: R^3 = 3-methoxypyridyl-5-methylamino; R^4 = F
52n: R^3 = 3-methoxypyridyl-5-methylamino; R^4 = H
52o: R^3 = tetrahydro-pyranyl-4-oxy; R^4 = Cl
52p: R^3 = tetrahydro-pyranyl-4-amino; R^4 = Cl
52q: R^3 = tetrahydro-pyranyl-4-aminomethyl; R^4 = Cl
52r: R^3 = *trans*-4-hydroxy-cyclohexylamino; R^4 = Cl
52s: R^3 = *cis*-4-hydroxy-cyclohexylamino; R^4 = Cl
52t: R^3 = *cis*-4-^{c}propyl-4-hydroxy-cyclohexylamino; R^4 = Cl
52u: R^3 = *trans*-4-hydroxy-cyclohexyloxy; R^4 = Cl
52v: R^3 = *cis*-4-hydroxy-cyclohexyloxy; R^4 = Cl

[a]Reagents and conditions: (a) Pd(PPh$_3$)$_4$, NaHCO$_3$, H$_2$O/1,4-dioxane, 150 °C, 5−30 min, microwave.

Meanwhile, the Janssen/Addex mGlu$_2$ PAM 1-butyl-3-chloro-4-(4-phenyl-1-piperidinyl)-(1H)-pyridone (**6**, JNJ-40411813/ADX71149) met the primary objectives of safety and tolerability in an exploratory phase IIa study in schizophrenia. Moreover, patients treated with antipsychotics who experience residual negative symptoms were identified as the subgroup that may

potentially benefit from add-on treatment with **6**, although this is yet to be established in a formal proof-of-concept study. In addition, in a second phase IIa study with **6** as adjunctive therapy in patients having major depressive disorder (MDD) with significant anxiety symptoms, **6** did not meet the criterion for efficacy vs placebo. Although **6** showed efficacy signals on several

Table 1. Comparison of Kinetic Parameters of 7 Determined by Two Different Methods[a]

assay	K_D (nM)[b]	k_{on} (M^{-1} min^{-1})	k_{off} (min^{-1})	RT (min)
association and dissociation[c]	1.1 ± 0.22	(7.1 ± 0.43) × 10^7	0.080 ± 0.015	12.5 ± 2.3
competition association[d]	2.5 ± 0.71	(2.3 ± 0.60) × 10^7	0.058 ± 0.005	17.3 ± 1.6

[a]Values represent the mean ± SEM of at least three individual experiments performed in duplicate. [b]Kinetic K_D values, defined as $K_D = k_{off}/k_{on}$. [c]Association and dissociation rate constants of [^{3}H]-7 in a classical radioligand kinetic binding assay at 28 °C using SPA. [d]Association and dissociation rate constants of 7 measured in a competition association assay at 28 °C using SPA.

Table 2. Functional Activity (pEC$_{50}$), Affinity (pK$_i$), and Kinetic Parameters (k_{on}, k_{off}, RT) for Reference mGlu$_2$ PAMs 2−5

compd	pEC$_{50}$	pK$_i$[b]	k_{on} (M^{-1} min^{-1})[c]	k_{off} (min^{-1})[c]	RT (min)[c,d]	K_D (nM)[c,e]
2	7.03 ± 0.14[a]	7.22 ± 0.15	(4.6 ± 2.3) × 10^6	0.086 ± 0.022	11.6 ± 2.9	190 ± 100
3	6.97 ± 0.08[a]	7.10 ± 0.04	(1.2 ± 0.38) × 10^6	0.120 ± 0.020	8.4 ± 1.4	100 ± 36
4	7.1 ± 0.1[a]	7.58 ± 0.08	(1.7 ± 0.70) × 10^6	0.090 ± 0.015	11.1 ± 1.9	51 ± 22
5	6.25 ± 0.06	6.43 ± 0.03	(2.1 ± 0.65) × 10^5	0.128 ± 0.040	7.8 ± 2.4	600 ± 260

[a]As previously described by Farinha et al. (2015).[42] [b]As previously described by Doornbos et al. (2016).[39] [c]Values represent the mean ± SEM of at least three individual experiments. [d]RT = $1/k_{off}$. [e]Kinetic K_D values, defined as $K_D = k_{off}/k_{on}$.

anxiety and depression measures, the primary end point was not met and overall the results did not suggest efficacy for **6** as an adjunctive treatment for patients with MDD with significant anxious symptoms.[16−22]

To understand more about the key in vitro parameters that could drive in vivo efficacy, we have focused on the ligand binding kinetics in addition to more classical in vitro parameters. It is now becoming increasingly apparent that in vivo efficacy can depend on optimized kinetic behavior.[23] Indeed, in the past decade the concept of ligand binding kinetics has received an increasing amount of interest.[24−27] Both the association and dissociation rate constants k_{on} and k_{off} have been studied for various drug targets including GPCRs.[28] The relevance of residence time (RT), defined as the reciprocal of the dissociation rate constant (RT = $1/k_{off}$), for in vivo efficacy was retrospectively shown for multiple marketed GPCR drugs, such as the long acting M$_3$ receptor antagonist tiotropium and fast dissociating D$_2$ antagonists with lower side-effect burden.[29−31] Whereas dissociation rates have been the focus of most kinetic studies, association rates have also been described to be important for fast drug action and high receptor occupancy.[32−34]

Here, we report the synthesis and biological evaluation of a novel series of 7-aryl-1,2,4-triazolo[4,3-a]pyridines, which evolved from a pyridone series (**4** and **6**) through a scaffold hopping drug-design strategy previously described.[35,36] These compounds were characterized as mGlu$_2$ PAMs in a functional assay, and additionally, radioligand binding experiments were performed to determine their affinity and kinetic binding parameters. We demonstrate that the differentiated binding kinetics result in a varied response in a label-free assay on whole cells. In this way we have been able for the first time to obtain both structure−activity/affinity relationships and structure−kinetic relationships for a class C GPCR.

■ CHEMISTRY

The target compounds **8−48** were prepared via Suzuki cross coupling of the corresponding 7-halotriazolopyridines (**49a,b**; **50a−c**; and **51a,b**) with an array of boronic esters (**52a−v**) as shown in Scheme 1. The chemical structures of compounds **8−48** are shown in Tables 3−6).

The key 7-halotriazolopyridines (**49a,b**; **50a−c**; and **51a,b**) and noncommercially available boronic esters (**52a−v**) were prepared following the procedures previously described.[37,38]
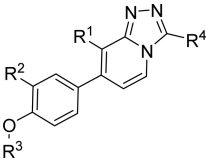
■ BIOLOGY

The potency of the compounds was determined by quantifying the increase in response of a fixed EC$_{20}$ glutamate concentration (4 μM) observed in a functional [^{35}S]GTPγS binding assay. The affinity of all compounds was determined in a full curve radioligand displacement assay in the presence of 6 nM of the mGlu$_2$ PAM 3-(cyclopropylmethyl)-7-[(4-phenyl-1-piperidinyl)methyl]-8-(trifluoromethyl)-1,2,4-triazolo[4,3-a]-pyridine (**7**, JNJ-46281222), which was radioactively labeled with tritium.[39] In order to determine the kinetic parameters k_{on} and k_{off}, we performed a radioligand competition association assay characterized by the equations of Motulsky and Mahan that describe the binding between two ligands competing for the same receptor binding site.[40] For this purpose, first the association rate constant k_{on} and dissociation rate constant k_{off} of **7** were determined in radioligand association and dissociation experiments using a scintillation proximity assay (SPA).[41] Kinetic parameters were determined at 28 °C; presumably these will increase at 37 °C. All kinetic assays were performed in the presence of 1 mM glutamate; this condition induced a monophasic association process of the PAM, which is required for the determination of the kinetic parameters of unlabeled PAMs.[39] The presence of glutamate was shown to not affect affinity and kinetic parameters of **7**.[39] Ultimately, three compounds with representative RT values were selected for comparison in a label-free, impedance based assay (xCELLigence) which measures ligand-induced responses on whole cells. This assay provided further understanding of the influence of RT on the duration of PAM-induced receptor activation.

■ RESULTS AND DISCUSSION

Kinetic rate constants k_{on} and k_{off} for **7** were similar when obtained in the association and dissociation assays compared to the competition association assay (Table 1), which validated the use of the competition association assay for all other compounds. Kinetic K_D values were comparable to the values reported before.[39]

Reference mGlu$_2$ PAMs **2−5** (Table 2) showed moderate to good potency and affinity at the mGlu$_2$ receptor, in agreement with previous reports.[39,42,43] Kinetic parameters k_{on}, k_{off}, and RT were also determined. Reference compound **2** was shown to have a RT of 11.6 min. The other reference PAMs had RTs in the same range, from 7.8 min for **5** to 17.3 min for **7** (Table 1).

Table 3. Functional Activity (pEC$_{50}$), Affinity (pK_i), and Kinetic Parameters (k_{on}, k_{off}, RT) for mGlu$_2$ PAMs 8−23

	R^1	R^2	R^3	R^4	pEC$_{50}$[a]	pK_i[b]	k_{on} (M^{-1} min^{-1})[c]	k_{off} (min^{-1})[d]	RT (min)[e]	K_D (nM)[f]
8	Cl	F	(structure)	CH$_2$-(c-Pr)	7.39 (7.35;7.43)	8.71 ± 0.12	(6.3 ± 1.5) x 10^6	0.097 ± 0.024	10.3 ± 2.5	15.3 ± 5.3
9	CF$_3$	F	(structure)	CH$_2$-(c-Pr)	8.06 ± 0.14	8.59 ± 0.10	(1.3 ± 0.49) x 10^7	0.033 ± 0.009	30.1 ± 8.2	2.5 ± 1.2
10	Me	F	(structure)	CH$_2$-(c-Pr)	7.11 (7.02; 7.19)	7.66 ± 0.33	(8.6 ± 3.3) x 10^6	0.086 ± 0.013	11.6 ± 1.8	10.0 ± 4.1
11	i-Pr	F	(structure)	CH$_2$-(c-Pr)	7.55 (7.55; 7.54)	7.60 ± 0.24	(6.5 ± 1.4) x 10^6	0.070 ± 0.017	14.2 ± 3.5	10.7 ± 3.5
12	Cl	Cl	(structure)	CH$_2$-(c-Pr)	7.91 (7.71; 8.11)	8.22 ± 0.13	(6.2 ± 2.4) x 10^7	0.061 ± 0.009	16.3 ± 2.4	1.0 ± 0.40
13	CF$_3$	Cl	(structure)	CH$_2$-(c-Pr)	8.54 (8.31; 8.78)	8.82 ± 0.22	(6.1 ± 2.4) x 10^6	0.044 ± 0.006	22.7 ± 2.9	7.3 ± 3.0
14	Me	Cl	(structure)	CH$_2$-(c-Pr)	7.76 ±0.26	7.83 ± 0.25	(5.5 ± 1.7) x 10^6	0.096 ± 0.021	10.5 ± 2.3	17.4 ± 6.5
15	Cl	F	(structure)	CH$_2$-(c-Pr)	6.60 (6.64; 6.55)	7.20 ± 0.14	(2.6 ± 0.72) x 10^6	0.096 ± 0.031	10.4 ± 3.4	37.6 ± 16
16	CF$_3$	F	(structure)	CH$_2$-(c-Pr)	7.25 ± 0.32	8.15 ± 0.05	(9.8 ± 5.2) x 10^6	0.090 ± 0.015	11.1 ± 1.8	9.2 ± 5.1
17	Cl	F	(structure)	CH$_2$-(c-Pr)	7.00 ± 0.10	7.73 ± 0.08	(3.0 ± 0.97) x 10^6	0.069 ± 0.011	14.4 ± 2.3	23.3 ± 8.4
18	CF$_3$	F	(structure)	CH$_2$-(c-Pr)	7.19 ± 0.10	8.00 ± 0.16	(8.3 ± 0.60) x 10^6	0.095 ± 0.020	10.5 ± 2.2	11.5 ± 2.5
19	Cl	F	(structure)	CH$_2$-(c-Pr)	7.06 ± 0.07	7.27 ± 0.20	(1.7 ± 0.82) x 10^6	0.073 ± 0.004	13.7 ± 0.8	42.7 ± 21
20	CF$_3$	F	(structure)	CH$_2$-(c-Pr)	7.73 ± 0.14	8.44 ± 0.07	(2.2 ± 0.42) x 10^7	0.189 ± 0.082	5.3 ± 2.3	8.6 ± 4.1
21	Cl	F	(structure)	CH$_2$-CF$_3$	7.53 ± 0.11	8.10 ± 0.24	(2.9 ± 0.49) x 10^7	0.096 ± 0.013	10.5 ± 1.5	3.3 ± 0.7
22	Cl	F	(structure)	CH$_2$-OEt	7.13 (7.27; 6.99)	8.19 ± 0.10	(3.0 ± 0.11) x 10^6	0.076 ± 0.004	13.2 ± 0.7	25.2 ± 1.6
23	CF$_3$	F	(structure)	CH$_2$-OEt	7.53 ± 0.19	7.93 ± 0.26	(3.6 ± 2.1) x 10^7	0.075 ± 0.006	13.4 ± 1.0	2.1 ± 1.2

[a]Values represent the mean followed by individual values in parentheses when of two experiments and the mean ± SEM when of three or more experiments. [b,c,d,e,f]Values represent the mean ± SEM of at least three individual experiments, all performed in duplicate. [e]RT = 1/k_{off}. [f]Kinetic K_D values, defined as K_D = k_{off} / k_{on}.

The analysis of the triazolopyridines containing a substituted pyridine (Table 3) began with elaboration of the R^1 substitution. Compound **8** was taken as the starting point. Substitution of chlorine at the R^1 position by trifluoromethyl (**9**) resulted in an increase in potency, while affinity remained the same. Introduction of methyl (**10**) or isopropyl (**11**) led to an approximately 10-fold decrease in affinity and potency. Interestingly both k_{on} and RT values were similar for **8**, **10**, and **11** but 2-fold (k_{on}) and approximately 3-fold (RT) higher for **9**. Substitution of fluorine by chlorine at the R^2 position resulted in increased potency and affinity for **12**, **13**, and **14**. In both cases, the PAMs with CF$_3$ at R^1 (**9** and **13**) showed modestly longer

Table 4. Functional Activity (pEC_{50}), Affinity (pK_i), and Kinetic Parameters (k_{on}, k_{off}, RT) for mGlu$_2$ PAMs 24−30
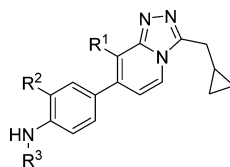
compd	R^1	R^2	R^3	pEC_{50}[a]	pK_i[b]	k_{on} (M^{-1} min^{-1})[b]	k_{off} (min^{-1})[b]	RT (min)[b,c]	K_D (nM)[b,d]
24	Cl	F	i-Pr	6.65 (6.43; 6.88)	7.21 ± 0.07	$(5.0 ± 1.2) × 10^6$	0.101 ± 0.009	9.9 ± 0.9	20.3 ± 5.4
25	CF$_3$	F	i-Pr	7.03 (7.44; 6.62)	8.05 ± 0.10	$(4.6 ± 1.1) × 10^7$	0.100 ± 0.029	10.0 ± 2.9	2.2 ± 0.8
26	CF$_3$	Cl	i-Pr	7.76 (7.55; 7.96)	8.41 ± 0.07	$(3.6 ± 1.3) × 10^7$	0.121 ± 0.035	8.2 ± 2.4	3.4 ± 1.6
27	Cl	F	c-Pr	7.20 (7.19; 7.21)	7.99 ± 0.05	$(4.8 ± 1.5) × 10^6$	0.061 ± 0.006	16.4 ± 1.7	12.7 ± 4.1
28	CF$_3$	F	c-Pr	7.52 (7.60; 7.43)	8.44 ± 0.07	$(7.7 ± 4.8) × 10^7$	0.086 ± 0.018	11.9 ± 2.3	1.1 ± 0.7
29	CF$_3$	Cl	c-Pr	8.11 (8.04; 8.18)	8.65 ± 0.11	$(7.7 ± 3.8) × 10^7$	0.088 ± 0.007	11.3 ± 0.9	1.2 ± 0.6
30	Cl	Cl	c-Pr	7.53 (7.54; 7.51)	8.17 ± 0.03	$(1.4 ± 0.35) × 10^7$	0.084 ± 0.016	11.9 ± 2.3	6.1 ± 1.9

[a]Values represent the mean followed by individual values in parentheses. [b]Values represent the mean ± SEM of at least three individual experiments. [c]RT = $1/k_{off}$. [d]Kinetic K_D values, defined as $K_D = k_{off}/k_{on}$.

Table 5. Functional Activity (pEC_{50}), Affinity (pK_i), and Kinetic Parameters (k_{on}, k_{off}, RT) for mGlu$_2$ PAMs 31−35
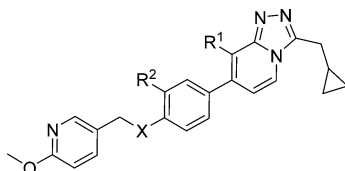
compd	R^1	R^2	X	pEC_{50}[a]	pK_i[b]	k_{on} (M^{-1} min^{-1})[b]	k_{off} (min^{-1})[b]	RT (min)[b,c]	K_D (nM)[b,d]
31	CF$_3$	F	O	7.39 (7.40; 7.37)	7.93 ± 0.14	$(1.1 ± 0.40) × 10^7$	0.173 ± 0.007	5.8 ± 0.2	16.0 ± 5.9
32	CF$_3$	H	O	7.24 ± 0.07	8.06 ± 0.16	$(1.4 ± 0.86) × 10^7$	0.125 ± 0.013	8.0 ± 0.8	8.7 ± 5.4
33	CF$_3$	F	NH	8.23 (8.13; 8.33)	8.69 ± 0.16	$(1.5 ± 0.94) × 10^7$	0.044 ± 0.005	22.7 ± 2.8	2.9 ± 1.9
34	CF$_3$	H	NH	7.82 ± 0.05	8.50 ± 0.09	$(3.4 ± 1.3) × 10^7$	0.069 ± 0.012	14.6 ± 2.6	2.0 ± 0.8
35	Cl	H	NH	6.82 (6.94; 6.71)	8.13 ± 0.08	$(6.2 ± 1.6) × 10^6$	0.097 ± 0.022	10.3 ± 2.3	15.6 ± 5.3

[a]Values represent the mean followed by individual values in parentheses when of two experiments and the mean ± SEM when of three or more experiments. [b]Values represent the mean ± SEM of at least three individual experiments, all performed in duplicate. [c]RT = $1/k_{off}$. [d]Kinetic K_D values, defined as $K_D = k_{off}/k_{on}$.

RTs of 30 and 23 min, respectively, along with highest potency and affinity.

Exploration of the pyridine R^3 revealed the importance of the position of the nitrogen. Compound **15** showed decreased potency and affinity compared to **8**. A similar trend was seen for **16** that showed values comparable to those reported previously which revealed decreased potency and affinity compared to **9**.[42] Values for k_{on} followed this trend, whereas RTs remained the same for **15** but decreased from 30 to 11 min for **16**. Subsequently the alkyl substituents on the pyridine ring were evaluated. Substitution of methyl in **15** by ethyl in **17** led to an increased potency and affinity. Addition of a methyl group on the 5-position of **16** did not change affinity or potency in **18**, nor were large changes seen in kinetic parameters. Introduction of the bulky and lipophilic isopropyl in **19** and **20** increased potency, affinity, and k_{on} slightly. Interestingly, the RT of **20** was reduced to only 5 min.

Substitution of the cyclopropylmethyl substituent at the R^4 position by 2,2,2-trifluoroethyl (**21**) resulted in a slight decrease in affinity, similar values for potency and RT, and a 5-fold increase in k_{on} compared to **8**. Next, the ethoxymethyl substituent was evaluated at R^4 (**22**), which yielded a slight decrease in potency, a 10-fold decrease in k_{on}, and similar values for affinity and RT compared to **21**. Substitution of F in **22** by CF$_3$ at R^1 did not yield a drastic increase in affinity and potency (**23**). Together, **21**−**23** showed that a cyclopropylmethyl

substituent at R^4 is preferred, as in all three cases the analogue bearing cyclopropylmethyl at R^4 showed a higher affinity (**8** or **9**).

The structure of substituted pyridine of **8** was changed to the short aliphatic isopropyl or cyclopropyl substituent, yielding **24**−**30** (Table 4). Potency and affinity of **24** were relatively low (pEC_{50} = 6.65; pK_i = 7.21). Changing the R^1 substituent to CF$_3$ (**25**) increased affinity and potency again (pEC_{50} = 7.03; pK_i = 8.05). Substitution of the fluorine on R^2 to chlorine (**26**) resulted in a ~3-fold increase in affinity and potency.

Substitution of i-Pr at the R^3 position by a c-Pr induced an increase in affinity and potency in all cases (**27**−**29**). As observed in Table 3, replacing F at R^2 in **27** by Cl in **30** led to an increased affinity and potency and a concomitant increase in k_{on}. The data in Table 4 show that k_{on} values followed affinity, whereas RT values were all within a narrow range (8.2−11.9 min).

In addition to the results obtained with the first subseries of triazolopyridines **8**−**23**, a 4-methoxy-3-pyridine moiety connected by a methylene spacer was introduced, leading to compounds **31**−**35** (Table 5). These molecules share a moderate to good potency and affinity (pEC_{50} = 6.8−7.8; pK_i = 7.9−8.7). Removal of the fluorine at the R^2 position (**32**) did not significantly change affinity, potency, or kinetic parameters when compared to **31**. Changing the ether linker in **31** and **32** to an amine in **33** and **34** resulted in an approximately 3-fold increase in affinity and potency. A moderate increase in k_{on} was observed

Table 6. Functional Activity (pEC$_{50}$), Affinity (pK$_i$), and Kinetic Parameters (k_{on}, k_{off}, RT) for mGlu$_2$ PAMs 36−48
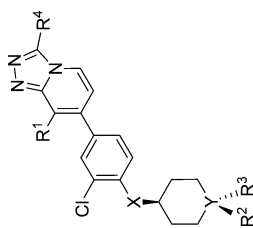
compd	R^1	R^2	R^3	R^4	X	Y	pEC$_{50}$[a]	pK$_i$[b]	k_{on} (M^{-1} min^{-1})[b]	k_{off} (min^{-1})[b]	RT (min)[b,c]	K$_D$ (nM)[b,d]
36	Cl			CH$_2$-(c-Pr)	O	O	6.65 (6.54; 6.77)	7.64 ± 0.01	(3.3 ± 1.4) × 10^6	0.092 ± 0.014	10.9 ± 1.7	28.1 ± 13
37	CF$_3$			CH$_2$-(c-Pr)	O	O	7.42 (7.40; 7.45)	8.28 ± 0.18	(2.0 ± 0.61) × 10^7	0.241 ± 0.063	4.1 ± 1.1	12.3 ± 5.0
38	Cl			CH$_2$-(c-Pr)	NH	O	6.83 (6.77; 6.89)	7.41 ± 0.21	(7.0 ± 2.4) × 10^6	0.136 ± 0.023	7.3 ± 1.2	19.5 ± 7.5
39	CF$_3$			CH$_2$-(c-Pr)	NH	O	7.73 (7.77; 7.68)	8.30 ± 0.06	(1.8 ± 0.61) × 10^7	0.067 ± 0.008	15.0 ± 1.8	3.8 ± 1.4
40	CF$_3$			CH$_2$-(c-Pr)	CH$_2$-NH	O	6.20 (6.23; 6.18)	7.21 ± 0.06	(1.7 ± 0.18) × 10^6	0.091 ± 0.018	11.0 ± 2.1	54 ± 12
41	Cl	H	OH	CH$_2$-(c-Pr)	NH	C	7.48 ± 0.22	8.52 ± 0.08	(6.7 ± 1.3) × 10^6	0.084 ± 0.011	11.8 ± 1.6	12.7 ± 3.0
42	CF$_3$	H	OH	CH$_2$-(c-Pr)	NH	C	8.03 ± 0.12	8.66 ± 0.01	(1.1 ± 0.09) × 10^7	0.033 ± 0.002	30.8 ± 1.7	3.0 ± 0.3
43	CF$_3$	OH	H	CH$_2$-(c-Pr)	NH	C	7.38 ± 0.08	8.03 ± 0.17	(5.7 ± 1.3) × 10^6	0.058 ± 0.014	17.1 ± 4.0	10.3 ± 3.4
44	CF$_3$	OH	c-Pr	CH$_2$-(c-Pr)	NH	C	8.95 (9.00; 8.90)	9.05 ± 0.10	(1.4 ± 0.16) × 10^7	0.020 ± 0.005	49.5 ± 12.4	1.5 ± 0.4
45	Cl	H	OH	CH$_2$-CF$_3$	NH	C	7.38 (7.41; 7.34)	8.22 ± 0.20	(6.7 ± 1.3) × 10^6	0.074 ± 0.015	13.6 ± 2.8	10.8 ± 3.1
46	CF$_3$	OH	H	CH$_2$-(c-Pr)	O	C	7.60 (7.64; 7.57)	8.72 ± 0.15	(1.2 ± 0.31) × 10^7	0.036 ± 0.001	28.1 ± 0.7	3.0 ± 0.8
47	Cl	H	OH	CH$_2$-CF$_3$	O	C	6.80 (6.73; 6.88)	7.94 ± 0.04	(8.3 ± 3.6) × 10^6	0.137 ± 0.049	7.3 ± 1.2	16.6 ± 9.3
48	Cl	OH	H	CH$_2$-CF$_3$	O	C	7.01 (7.03; 6.99)	7.49 ± 0.21	(6.9 ± 1.5) × 10^6	0.056 ± 0.001	17.7 ± 0.2	8.1 ± 1.7

[a]Values represent the mean followed by individual values in parentheses when of two experiments and the mean ± SEM when of three or more experiments. [b]Values represent the mean ± SEM of at least three individual experiments, all performed in duplicate. [c]RT = 1/k_{off}. [d]Kinetic K_D values, defined as $K_D = k_{off}/k_{on}$.

and interestingly a 4- and 2-fold increase in RT for **33** and **34**, respectively. This may be explained by the increased flexibility given by the methylene bridge between the triazolopyridine core and the pyridine substituent. As seen in many examples, substitution of CF_3 in **34** to Cl in **35** led to a decrease in affinity, potency, and kinetic parameter values.

Reducing aromaticity and introducing more aliphatic and sp^3 character can sometimes be beneficial for physicochemical properties and druglikeness.[44] In order to evaluate the effects of aromaticity, the 4-methoxy-3-pyridyl substituent was replaced with a 4-tetrahydropyranyl ring (**36**, Table 6). This change resulted in a pK_i and potency (pEC_{50}) of 6.65 and 7.64, respectively, which were increased in **37** by the introduction of CF_3 in the R^1 position. Compound **37** has a high affinity (pK_i = 8.28) and increased k_{on} (2.0×10^7 M^{-1} min^{-1}); however, contrary to the high affinity, its RT (4.1 min) was the shortest found throughout this study. As seen in the first series of ligands (Table 2), affinity and potency did not change by altering the linker atom from ether to amine (**38**, **39**). Increasing the linker length by a single methylene unit resulted in an approximately 10-fold loss in affinity, (**40**; pK_i = 7.21). Values for k_{on} followed affinity, but RT values were all in the same range.

The tetrahydropyran moiety was then replaced by a cyclohexanol ring, leading to **41**−**48**. Again, compounds bearing CF_3 at R^1 (**42**, **46**) showed better affinity and potency than their chlorine analogues (**41**, **45**). Molecule **42** showed not only a high potency (pEC_{50} = 8.03), affinity (pK_i = 8.66), and k_{on} (1.1×10^7 $M^{-1}min^{-1}$) but also a longer RT of 31 min. Its cis-diastereomer **43** showed a 3-fold reduction in potency (pEC_{50} = 7.38) and affinity (pK_i = 8.03), a 2-fold reduction in k_{on} (5.7×10^6 M^{-1} min^{-1}), and a small reduction in RT (17 min). Introduction of a c-Pr substituent at R^3 (**44**) led to an increase in potency (pEC_{50} = 8.95), affinity (pK_i = 9.05), and k_{on} (1.4×10^7 $M^{-1}min^{-1}$) and also to a prolonged RT of 50 min, which was the highest value observed in this study. It may be that the cyclopropyl at R^3 directs the hydrophilic hydroxyl into a better position for interaction with the receptor. Changing R^4 from c-Pr to CF_3 (**45**) did not change any parameter compared to **41**. Changing the linker group from amine in **43** to ether in **46** did not affect affinity and potency. However, RT seemed to be somewhat increased. Differences between diastereomers were seen again in **47** and **48**. Whereas the potencies were similar, affinity was decreased 3-fold and k_{on} remained similar, while RT was prolonged by 2-fold when moving from a trans to cis configuration.

In general, CF_3 was shown to be the preferred substituent at R^1. Compounds bearing this substituent typically had a higher potency and affinity. Interestingly, all PAMs with a RT longer than 20 min bear this moiety, including **44** with the longest RT seen in this study (50 min). On the other hand, molecule **37** had the shortest RT (4.1 min) and also contains the CF_3 group, indicating that CF_3 in itself is not the driver for long RT. At the R^2 position chlorine was shown to be the best substituent for high potency and affinity. PAMs bearing a substituted pyridine revealed the importance of its substitutions in combination with the position of the nitrogen in the ring for potency, affinity, and kinetic parameters.

The rather small differences in RT induced by substitutions at the R^1 and R^2 positions at the central triazolopyridine core indicated that this region does not induce large differences in RT. On the other hand, small differences in the distal tail of the compounds induced large differences in RT. As we have shown previously, this triazolopyridine series binds with the scaffold and R^4 substituent in the deepest part of the receptor, while the distal

tail points to the extracellular side.[39] These differences in RT may be explained by the tight receptor−ligand interactions of the triazolopyridine core compared to looser interactions on the extracellular side. Certain molecules may trap the more flexible ECL2 (or the tops of TMs 3 and 5) in conformations leading to longer RT. Such induced fit modulation of RT can involve ordering of loops to partially block the binding pocket and prevent ligand escape. This mechanism has been seen for multiple targets from different classes, among which the 5-HT$_{2B}$ receptor as reported in the recently published LSD-bound crystal structure.[24,45] Selectivity of this series of mGlu$_2$ PAMs for other members of the mGlu family was good. Representatives (**12**, **27**, **37**, and **45**) showed no activity at mGlu1, -3, -4, -5, -6, -7, or -8; see Supporting Information Table S1.

In order to compare the kinetic parameters and affinity, a kinetic map was generated (Figure 2). In this map k_{on} (x-axis), k_{off}
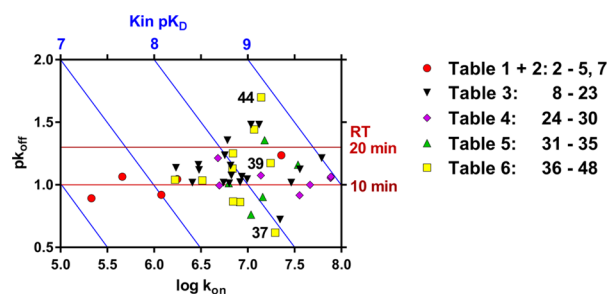

Figure 2. Kinetic map of all tested compounds. The dissociation rate (pk_{off}; k_{off}, min^{-1}) is plotted on the y-axis; the association rate (log k_{on}; k_{on}, M^{-1} min^{-1}) is on the x-axis. Identical affinity (pK_D) values may result from a different combination of k_{on} and k_{off} ($K_D = k_{off}/k_{on}$, diagonal blue lines). Horizontal lines indicating a RT of 10 and 20 min divide the compounds into short, medium, and long RT.

(y-axis), and K_D (diagonal lines) were plotted. Whereas k_{off} values were all within a small range of about 1 order of magnitude between 0.020 min^{-1} (**44**) and 0.241 min^{-1} (**37**), k_{on} values were more diverse and were spread over almost 2 orders of magnitude between 1.7×10^6 M^{-1} min^{-1} (**40**) to 7.7×10^7 M^{-1} min^{-1} (**28** and **29**). The molecules were plotted per subgroup, as presented in the different tables. This revealed that **8**−**23** and **24**−**30** were mostly diverse in on-rates (**8**−**23**, $(0.17-6.2) \times 10^7$ M^{-1} min^{-1}; **24**−**30**, $(0.48-7.7) \times 10^7$ M^{-1} min^{-1}), whereas **31**−**35** and **36**−**48** were more diverse in off-rates (**31**−**35**, 0.044−0.17 min^{-1}; **36**−**48**, 0.020−0.24 min^{-1}), indicating that an increased affinity between close analogues may be achieved by optimizing one kinetic parameter at a time. Interestingly, the five reference mGlu$_2$ PAMs **2**−**5** and **7**, which are very diverse in structure and affinity, differed mostly in terms of on-rate ($(0.21-4.6) \times 10^6$ $M^{-1}min^{-1}$), whereas off-rates were very close (0.086−0.13 min^{-1}). As expected, the compounds with the highest affinity either have a long RT (**44**) or a fast k_{on} (**28**, **29**). Ideally, these optimized parameters may be combined leading to an mGlu$_2$ PAM with even more increased affinity, which would be represented in the top right corner of the kinetic map. For further comparison, the compounds were arbitrarily divided into short RT (RT < 10 min), medium RT (10−20 min,) and long RT (>20 min) (Figure 2).

To gain more insight into the relationships between the different parameters studied, correlation plots were made (Figure 3). First, the affinity (pK_i) and potency (pEC_{50}) were shown to be linearly correlated (Figure 3A). Second, the affinity obtained from the classical radioligand displacement assay (pK_i) and
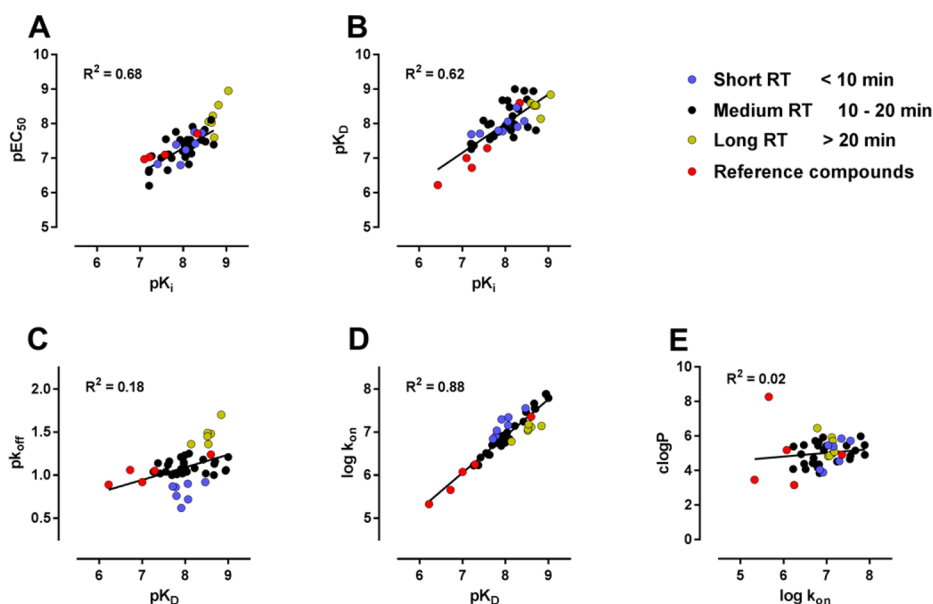
Figure 3. Correlation between affinity (pK_i) and potency (pEC_{50}) (A); affinity determined from [^{3}H]-**7** displacement assays (pK_i) and affinity determined based on kinetic parameters k_{on} and k_{off} obtained from [^{3}H]-**7** competition association experiments (pK_D) (B); affinity (pK_D) and dissociation rate (pk_{off}) (C); affinity (pK_D) and association rate ($\log k_{on}$) (D); association rate ($\log k_{on}$) and partition coefficient (clogP) (E).

affinity obtained from kinetic parameters (pK_D) were shown to be correlated (Figure 3B). This further supported the use of the kinetic SPA radioligand binding assay. Long RT PAMs were shown to share a high affinity and potency, but by itself a high potency or affinity does not predict a long RT (Figure 3A, Figure 3B, Figure S1). Then, the dissociation rate constants (pk_{off}) were plotted against the kinetic affinity data (pK_D) (Figure 3C), which did not show correlation. Interestingly, the association rate constants ($\log k_{on}$) were strongly correlated to affinity (pK_D) (Figure 3D). These parameters were both within a similar range of roughly 2 orders of magnitude for the compounds of our series. Interestingly, although having different structures and in some cases lower affinities and k_{on} values, the reference mGlu$_2$ PAMs (**2−5**) also fitted well in this correlation (Figure 3D). This indicated that this correlation has likely revealed a general trend for PAMs and how they bind at the mGlu$_2$ receptor.

Correlations between kinetic parameters and affinity have been made before. Most of these studies found a correlation between k_{off} values and affinity or efficacy, for instance, on the M$_3$ and A$_{2A}$ receptors.[46−48] However, a correlation between association rate constants and affinity, as was shown here for mGlu$_2$ PAMs, has also been observed before. Exemplary GPCRs are the OX$_2$ receptor and β_2-adrenoreceptors[49,50] and other targets such as the hERG channel.[51,52] These correlations are receptor-specific and may therefore be caused by differences in receptor structure, dynamics, or local environment of the receptor.

Recent simulation studies have stipulated the importance of fast association rates for receptor occupancy and drug dosing.[33,53] One of the mechanisms that may be responsible for these effects is receptor rebinding, which is described as the binding of freshly dissociated ligands from the local environment of the receptor.[54] These high local concentrations may lead to a prolonged activity of the drug, even when concentrations within the effect compartment have fallen below therapeutic levels.[55] For the mGlu$_2$ receptor, rebinding may play a role. The physiological synaptic environment of the receptor may permit more rebinding as its interstitial location will result in less

diffusion and therefore higher local ligand concentrations.[56,57] Another reason for receptor rebinding would be binding of compound to or in the cell membrane close to the receptor which may then act as a repository and facilitate the approach of the compound to the receptor.[56] This would, however, require a correlation between lipophilicity and association rate constants, as lipophilic compounds are more likely to bind to the cell membrane. Since the plot in Figure 3E shows no such correlation for the studied mGlu$_2$ PAMs, membrane binding is not likely to be involved for these compounds.

xCELLigence. We used a label-free, impedance-based technology (xCELLigence) to evaluate whether a long receptor binding RT leads to a prolonged functional activity. This method is based on the measurement of cellular impedance, expressed as cell index, and enables real-time recordings.[58] Responses induced by compound addition can thus be measured and quantified. Earlier studies have shown that results obtained were comparable to more classical end point assays.[59] As the assay is performed on whole cells at 37 °C, it is considered a valuable translational step toward in vivo experiments.[60] Endogenous glutamate levels at the time of experiments were around 90 μM. Compound-induced responses therefore represent the PAM effects. As a control, reference compound **7** was used to check the response on CHO-K1 WT cells compared to CHO-K1_hmGlu$_2$ cells (Figure S2). No response was found on the WT cells, indicating that the responses were mGlu$_2$ receptor-mediated. For further experiments we selected compounds with diversity in RT (measured at 28 °C): **37** (4.1 min), its close analogue **39** with 3- to 4-fold longer RT (15 min), and **44** with again a 3-fold longer RT compared to **39** (50 min; Figure 4A−D). We determined their potency in the label-free assay using CHO-K1_hmGlu$_2$ cells and found pEC_{50} values of 7.05 ± 0.04, 7.73 ± 0.23 and 7.95 ± 0.12, respectively. Then we performed a wash-out assay in order to evaluate differences in compound-induced responses after washing. This enabled us to trace the remaining response exerted by only receptor-bound compound. To this end we first determined the EC$_{80}$ concentrations of short RT **37**, medium RT **39**, and long RT **44**, which were 600, 200, and 60 nM,
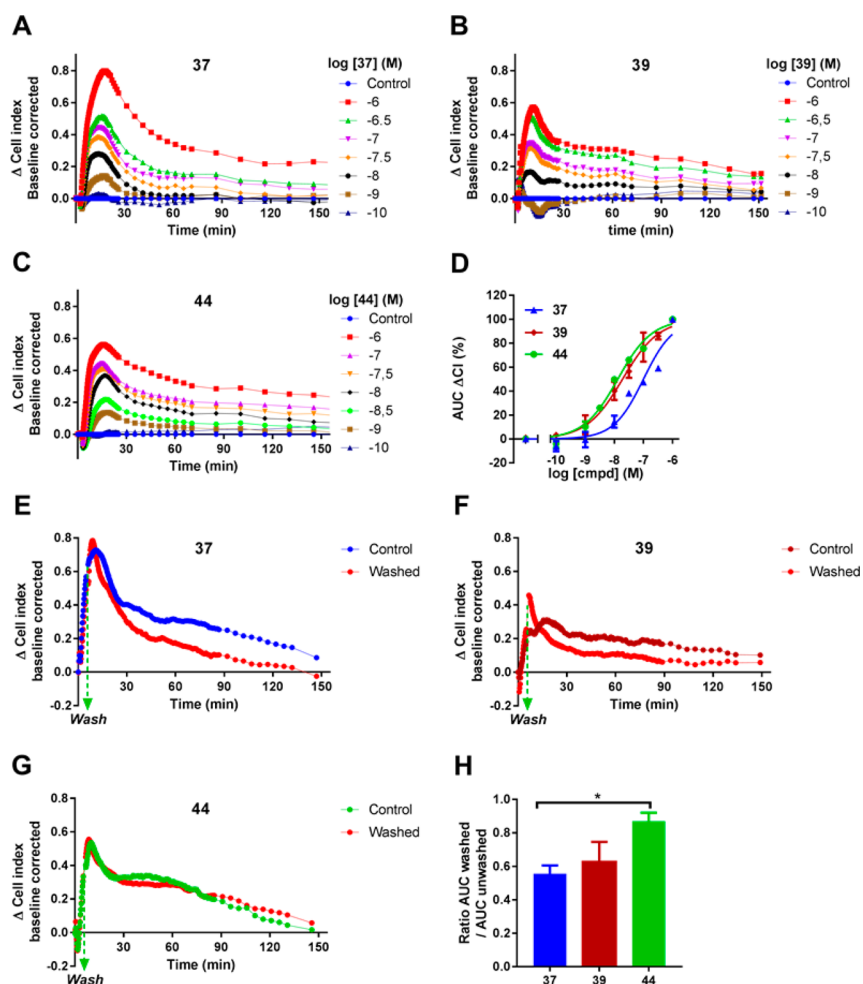
Figure 4. Concentration-dependent effects of **37** (A), **39** (B), and **44** (C) on CHO-K1 cells stably expressing the human mGlu$_2$ receptor. A representative example is shown of a baseline-corrected response, which was repeated three times in duplicate. (D) Concentration−effect curves of **37**, **39**, and **44**, derived from the AUC up to 150 min. Data are from three individual experiments performed in duplicate and are expressed as percentage of maximum AUC. Responses in a label-free, impedance-based assay induced by an EC$_{80}$ equivalent concentration of **37** (600 nM) (E), **39** (200 nM) (F), and **44** (60 nM) (G) with and without washing step induced 5 min after stimulation. A representative example is shown of a baseline-corrected response, which was repeated three times in duplicate. (H) Ligand-induced response that is left after washing step. Data are expressed as the ratio between the AUC of the trace of the washed and unwashed wells. Data are from three individual experiments performed in duplicate and are expressed as the mean ± SEM: (∗) $p < 0.05$.

respectively. Then, cells were stimulated with this EC$_{80}$ concentration, and just before maximal response was reached, after 5 min, cells were washed and fresh medium was added (Figure 4E−G). By comparing these traces with control traces of unwashed wells, we evaluated the differences in responses between **37**, **39**, and **44** as the ratio between the AUC of washed and unwashed wells (Figure 4H). The functional effect of **37** and **39** was partially lost in this experimental setup, while the effect of **44** remained almost unchanged. The wash-out assay showed a significant difference between short RT **37** and long RT **44**. The value for **39** was in between those of **37** and **44**, in agreement with its RT. Together, these data showed that a longer RT also leads to an increased functional effect under nonequilibrium conditions and that these parameters are positively correlated. Since equilibrium conditions are not always present in physiological conditions, these findings may be considered a translational step from in vitro toward in vivo experiments.

In Vivo Sleep−Wake Effects. Glutamate neurotransmission plays a key role in sleep−wake mechanisms, and these processes have translational value for central activity and target engagement. Previous in vivo studies have repeatedly shown that positive allosteric modulation of the mGlu$_2$ receptor results in distinct changes in rodent sleep−wake organization, more specifically in a dose-dependent reduction in so-called rapid eye movement sleep or REM sleep.[61,62] Changes in sleep−wake states in the rat are of a dynamic nature, i.e., with more frequent transitions between sleep−wake states as compared to humans: therefore the effects of mGlu$_2$ PAM compounds on REM sleep are expressed as averages over, for example, 2 or 4 h periods after compound administration. In order to investigate whether the different RT values are reflected in the sleep−wake related pharmacodynamic readout, sleep−wake analysis of **9** and **20** (selected as examples with long versus short in vitro RT, respectively, yet having appropriate and similar pharmacokinetic behavior) was even done on a 5 min basis to optimally capture sleep changes in function of time. All methods, (circadian) timings, and analyses otherwise were similar to those reported earlier by Ahnaou et al. (2016).[62]

Figure 5 shows the effects of **9** and **20** on REM sleep reduction in rats for 24 consecutive 5 min periods after a single oral administration of 1, 3, and 10 mg/kg and 20% CD vehicle control. The first 6 consecutive 5 min periods can be discarded due to the
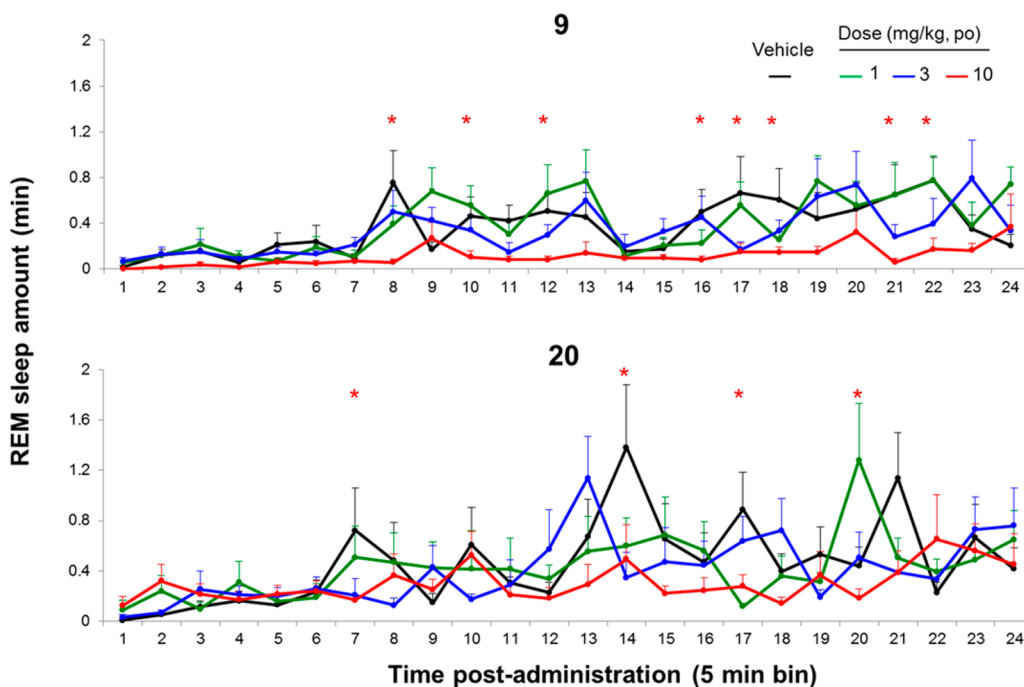
Figure 5. Average amount of REM sleep in minutes for 24 consecutive 5 min period during the first 2 h of the recording session after oral administration of **9** (top panel) and **20** (bottom panel), each at 1, 3, 10 mg/kg, po, to Sprague-Dawley rats ($n = 8$ for each condition). Black lines indicate control vehicle condition (20% CD), while the green, blue, and red lines indicate doses of 1, 3, 10 mg/kg, respectively. Error flags indicate SEM values: note that the higher time resolution of 5 min bins also causes REM sleep changes to be expressed more dynamically and less "consistent" as compared to reduction score averaged over the whole 2 h postadministration period. ∗ indicates $p < 0.05$ vehicle compared to 10 mg/kg, mixed model ANOVA.

confounding arousing effect of the oral administration procedure per se, the animal returning to undisturbed REM sleep baseline values after about 30 min. Molecule **9** showed a longer in vitro RT of 30 min, while for **20** it was 5 min. Correspondingly, at the higher dose of 10 mg/kg, the effect of **9** on REM reduction seemed more immediate and constant compared to **20**. For both compounds no effects on total sleep were seen (Figure S3).

Compounds **9** and **20** showed similar in vitro binding affinities with pK_i values of 8.59 and 8.44, respectively. At 10 mg/kg, estimated free levels in brain 1 h after administration are 5 and 3.5 ng/g for **9** and **20**, respectively. Hence the two molecules show similar affinity and roughly similar range of free concentrations in brain. While the underlying mechanism causing this different in vivo effect is still to be elucidated, this finding provides a first hint that different RTs may impact the in vivo effect. The interplay of RT with elimination/clearance from brain is important for the resulting in vivo effect, but with similar levels of **9** and **20** after 1 h, it seems that RT may play a role in this case. To strengthen these observations, future experiments could include the synthesis of PET ligands with different residence times and further in vivo studies with a different end point such as cognition.

While potent GPCR antagonists can act via a long RT with expected improved clinical efficacy, there is limited published data assessing the relationship between agonist/PAM RT and in vivo efficacy. Agonist responses are usually regulated by receptor desensitization and internalization, which can act to limit the effect and duration of receptor signaling. PAMs do not activate receptors in the absence of agonist, and hence allosteric modulators with prolonged action may not be negated by internalization and loss of function due to longer RT of the PAM−receptor complex.

CONCLUSIONS

In this study we described a series of 7-aryl-1,2,4-triazolo[4,3-a]pyridines with potent mGlu$_2$ PAM activity and a high affinity. An SPA radioligand binding assay was developed to study the kinetic parameters of these compounds. We showed that association rate constants range within 3 orders of magnitude, whereas RT values are more confined, from 4.1 min (**37**) up to 50 min (**44**). Correlation plots between affinity and kinetic parameters revealed a strong correlation between affinity and association rate constants, whereas no such correlation was found between RT and affinity.

Structure−kinetics relationships were explored in addition to the more traditional structure−activity/affinity relationships analysis. We learned that a CF$_3$ substituent at R^1 increased potency and affinity and was also important for RT but did not lead to a long RT per se as shown by its presence in **37** ("short" RT) and **44** ("long" RT). Chlorine was the preferred substituent for R^2, it increased potency and affinity but not RT. Differences in the distal tail of the molecules, such as small changes in the pyridine moiety or single substitutions to the cyclohexanol, induced the biggest differences in RT. This was exemplified by the introduction of c-Pr in **44**, leading to a 3-fold increase in RT compared to **43**.

To evaluate whether a long RT also leads to a prolonged functional effect, **37**, **39**, and **44** were evaluated in a wash-out assay using the label-free impedance based xCELLigence technique. The response of **44** on whole cells at physiological temperature remained more sustained after washing than that of **37** and **39**. These data suggested that an increased lifetime of the receptor−ligand complex (RT) is correlated to an increased functional effect under nonequilibrium conditions.

Together, these results show for the first time for a class C GPCR that optimization of ligand binding kinetics in addition to

potency and affinity is possible. Given that pure PAMs do not exert an effect in the absence of glutamate and are thus less likely to induce on-target toxicity, a long RT seems a promising strategy for these ligands. As rebinding may be involved in mGlu$_2$ receptor occupancy, a RT for **44** in our system of 50 min may be prolonged in the interstitial synaptic environment. Without any on-target toxicity occurring, the design of mGlu$_2$ PAMs with even longer RTs may be a logical next step. Lastly, a first attempt was made to relate the compound's RT to its in vivo pharmacodynamic effect. Ultimately, this study may contribute to the development of compounds with a high affinity and efficacy in vitro and in vivo, not only for the mGlu$_2$ receptor but also for other GPCRs.

■ EXPERIMENTAL SECTION

Chemistry. Unless otherwise noted, all reagents and solvents were obtained from commercial suppliers and used without further purification. Thin layer chromatography (TLC) was carried out on silica gel 60 F254 plates (Merck). Flash column chromatography was performed on silica gel, particle size 60 Å, mesh of 230−400 (Merck) under standard techniques. Microwave assisted reactions were performed in a single-mode reactor, Biotage Initiator Sixty microwave reactor (Biotage), or in a multimode reactor, MicroSYNTH Labstation (Milestone, Inc.). Nuclear magnetic resonance (NMR) spectra were recorded with either a Bruker DPX-400 or a Bruker AV-500 spectrometer (Bruker AG) with standard pulse sequences, operating at 400 and 500 MHz, respectively, using CDCl$_3$ and DMSO-d_6 as solvents. Chemical shifts (δ) are reported in parts per million (ppm) downfield from tetramethylsilane (δ = 0). Coupling constants are reported in hertz. Splitting patterns are defined by s (singlet), d (doublet), dd (double doublet), t (triplet), q (quartet), quin (quintet), sex (sextet), sep (septet), or m (multiplet). Liquid chromatography combined with mass spectrometry (LC−MS) was performed on either a HP 1100 HPLC system (Agilent Technologies) or Advanced Chromatography Technologies system composed of a quaternary or binary pump with degasser, an autosampler, a column oven, a diode array detector (DAD), and a column as specified in the respective methods below. Flow from the column was split to a MS spectrometer. The MS detector was configured with either an electrospray ionization source or an ESCI dual ionization source (electrospray combined with atmospheric pressure chemical ionization). Nitrogen was used as the nebulizer gas. Data acquisition was performed with MassLynx-Openlynx software or with Chemsation-Agilent data browser software. Melting point values are peak values and were obtained with experimental uncertainties that are commonly associated with this analytical method. Melting points were determined in open capillary tubes on a Mettler FP62 apparatus with a temperature gradient of 10 °C/min. Maximum temperature was 300 °C.

Purities of all new compounds were determined by analytical RP HPLC using the area percentage method on the UV trace recorded at a wavelength of 254 nm, and compounds were found to have ≥95% purity unless otherwise specified.

8-Chloro-3-cyclopropylmethyl-7-{4-[(2,6-dimethylpyridin-3-yl)oxy]-3-fluorophenyl}[1,2,4]triazolo[4,3-a]pyridine (8). To a stirred suspension of **50a** (1.7 g, 5.09 mmol) and **52a** (2.1 g, 6.12 mmol) in a saturated aqueous solution of NaHCO$_3$ (18 mL) and 1,4-dioxane (36 mL) was added Pd(PPh$_3$)$_4$ (0.589 g, 0.51 mmol). The mixture was heated at 150 °C for 10 min under microwave irradiation. The mixture was cooled to room temperature and filtered through a Celite pad. The filtrate was diluted with water (20 mL) and extracted with EtOAc (2 × 15 mL). The organic layer was washed with brine (15 mL), dried over anhydrous Na$_2$SO$_4$, and concentrated in vacuo. The crude was purified by flash column chromatography (silica gel, EtOAc in DCM, 0/100 to 20/80) to give the desired product **8** as a white solid (1.3 g, 60%). Mp 207.2 °C. ^{1}H NMR (500 MHz, CDCl$_3$) δ ppm 0.32−0.42 (m, 2H), 0.61−0.69 (m, 2H), 1.17−1.28 (m, 1H), 2.54 (s, 3H), 2.55 (s, 3H), 3.13 (d, J = 6.9 Hz, 2H), 6.87 (d, J = 6.9 Hz, 1H), 6.92 (t, J = 8.4 Hz, 1H), 7.02 (d, J = 8.4 Hz, 1H), 7.16 (d, J = 8.4 Hz, 1H), 7.25 (d, J = 9.2 Hz, 1H),

7.41 (dd, J = 11.3, 1.7 Hz, 1H), 7.98 (d, J = 6.9 Hz, 1H). LC−MS m/z 423 [M + H]$^+$, t_R = 2.86 min.

8-Trifluoromethyl-3-cyclopropylmethyl-7-{4-[(2,6-dimethyl-pyridin-3-yl)oxy]-3-fluorophenyl}[1,2,4]triazolo[4,3-a]pyridine (9). Starting from **49a** (0.150 g, 0.54 mmol) and **52a** (0.242 g, 0.707 mmol) and following the procedure described for **8**, compound **9** was obtained as a white solid (0.139 g, 56%). ^{1}H NMR (400 MHz, CDCl$_3$) δ ppm 0.31−0.43 (m, 2H), 0.61−0.70 (m, 2H), 1.16−1.30 (m, 1H), 2.53 (s, 3H), 2.55 (s, 3H), 3.15 (d, J = 6.7 Hz, 2H), 6.79 (d, J = 7.2 Hz, 1H), 6.89 (t, J = 8.3 Hz, 1H), 7.01 (d, J = 8.3 Hz, 1H), 7.05 (br d, J = 8.6 Hz, 1H), 7.14 (d, J = 8.3 Hz, 1H), 7.22 (dd, J = 10.9, 2.1 Hz, 1H), 8.11 (d, J = 7.2 Hz, 1H). LC−MS m/z 457 [M + H]$^+$, t_R = 3.03 min.

8-Methyl-3-cyclopropylmethyl-7-{4-[(2,6-dimethylpyridin-3-yl)oxy]-3-fluorophenyl}[1,2,4]triazolo[4,3-a]pyridine (10). Starting from **51a** (0.250 g, 1.127 mmol) and **52a** (0.464 g, 1.35 mmol) and following the procedure described for **8**, compound **10** was obtained as a white solid (0.103 g, 23%). Mp 147.4 °C. ^{1}H NMR (500 MHz, CDCl$_3$) δ ppm 0.32−0.39 (m, 2H), 0.60−0.67 (m, 2H), 1.16−1.29 (m, 1H), 2.55 (s, 6H), 2.65 (s, 3H) 3.11 (d, J = 6.65 Hz, 2H), 6.78 (d, J = 7.22 Hz, 1H), 6.93 (t, J = 8.38 Hz, 1H), 7.00 (d, J = 8.38 Hz, 1H), 7.07 (d, J = 8.38 Hz, 1H), 7.13 (d, J = 8.09 Hz, 1H), 7.23 (dd, J = 11.27, 2.02 Hz, 1H), 7.89 (d, J = 6.94 Hz, 1H). LC−MS m/z 403 [M + H]$^+$, t_R = 2.07 min.

8-Cyclopropyl-3-cyclopropylmethyl-7-{4-[(2,6-dimethylpyri-din-3-yl)oxy]-3-fluorophenyl}[1,2,4]triazolo[4,3-a]pyridine (11). Starting from **51b** (0.230 g, 0.93 mmol) and **52a** (0.382 g, 1.11 mmol) and following the procedure described for **8**, compound **11** was obtained as a white solid (0.269 g, 68%). Mp 166.4 °C. ^{1}H NMR (400 MHz, CDCl$_3$) δ ppm 0.29−0.38 (m, 2H), 0.58−0.67 (m, 2H), 0.90−1.00 (m, 2H), 1.14−1.31 (m, 1H), 1.55−1.70 (m, 2H) 2.10 (tt, J = 8.64, 5.46 Hz, 1H), 2.54 (s, 3H), 2.55 (s, 3H), 3.06 (d, J = 6.70 Hz, 2H), 6.73 (d, J = 7.17 Hz, 1H), 6.93 (t, J = 8.44 Hz, 1H), 7.00 (d, J = 8.32 Hz, 1H), 7.13 (d, J = 8.32 Hz, 1H), 7.15−7.20 (m, 1H), 7.32 (dd, J = 11.21, 1.97 Hz, 1H), 7.80 (d, J = 7.17 Hz, 1H). LC−MS m/z 429 [M + H]$^+$, t_R = 2.24 min.

8-Chloro-3-cyclopropylmethyl-7-{4-[(2,6-dimethylpyridin-3-yl)oxy]-3-chlorophenyl}[1,2,4]triazolo[4,3-a]pyridine (12). Starting from **50a** (0.250 g, 0.75 mmol) and **52b** (0.385 g, 0.75 mmol) and following the procedure described for **8**, compound **12** was obtained as a white solid (0.100 g, 70%). Mp 182.7 °C. ^{1}H NMR (400 MHz, CDCl$_3$) δ ppm 0.31−0.41 (m, 2H), 0.57−0.70 (m, 2H), 1.21−1.33 (m, 1H), 2.51 (s, 3H), 2.56 (s, 3H), 3.13 (d, J = 6.94 Hz, 2H), 6.82 (d, J = 8.55 Hz, 1H), 6.87 (d, J = 6.94 Hz, 1H), 7.03 (d, J = 8.32 Hz, 1H), 7.16 (d, J = 8.09 Hz, 1H), 7.37 (dd, J = 8.55, 2.31 Hz, 1H), 7.66 (d, J = 2.31 Hz, 1H), 7.97 (d, J = 7.17 Hz, 1H). LC−MS m/z 439 [M + H]$^+$, t_R = 3.08 min.

8-Trifluoromethyl-3-cyclopropylmethyl-7-{4-[(2,6-dimethyl-pyridin-3-yl)oxy]-3-chlorophenyl}[1,2,4]triazolo[4,3-a]pyridine (13). Starting from **49a** (0.2 g, 0.73 mmol) and **52b** (0.26 g, 0.72 mmol) and following the procedure described for **8**, compound **13** was obtained as a white solid (0.217 g, 61%). Mp > 300 °C. ^{1}H NMR (400 MHz, CDCl$_3$) δ ppm 0.34−0.41 (m, 2H), 0.62−0.70 (m, 2H), 1.16−1.30 (m, 1H), 2.50 (s, 3H), 2.56 (s, 3H), 3.15 (d, J = 6.70 Hz, 2H), 6.79 (d, J = 8.09 Hz, 2H), 7.03 (d, J = 8.09 Hz, 1H), 7.11−7.19 (m, 2H), 7.49 (d, J = 2.31 Hz, 1H), 8.10 (d, J = 7.17 Hz, 1H). LC−MS m/z 473 [M + H]$^+$, t_R = 3.22 min.

8-Methyl-3-cyclopropylmethyl-7-{4-[(2,6-dimethylpyridin-3-yl)oxy]-3-chlorophenyl}[1,2,4]triazolo[4,3-a]pyridine (14). Starting from **60a** (0.250 g, 0.127 mmol) and **52b** (0.464 g, 1.35 mmol) and following the procedure described for **8**, compound **14** was obtained as a white solid (0.107 g, 22%). Mp 121 °C. ^{1}H NMR (500 MHz, CDCl$_3$) δ ppm 0.36 (q, J = 5.01 Hz, 2H), 0.58−0.67 (m, 2H), 1.17−1.30 (m, 1H), 2.52 (s, 3H), 2.56 (s, 3H), 2.64 (s, 3H), 3.11 (d, J = 6.65 Hz, 2H), 6.78 (d, J = 6.94 Hz, 1H), 6.83 (d, J = 8.67 Hz, 1H), 7.02 (d, J = 8.38 Hz, 1H), 7.13 (d, J = 8.09 Hz, 1H), 7.18 (dd, J = 8.38, 2.02 Hz, 1H), 7.49 (d, J = 2.31 Hz, 1H), 7.89 (d, J = 6.94 Hz, 1H). LC−MS m/z 419 [M + H]$^+$, t_R = 2.23 min.

8-Chloro-3-cyclopropylmethyl-7-{4-[(2-methylpyridin-4-yl)-oxy]-3-fluororophenyl}[1,2,4]triazolo[4,3-a]pyridine (15). Starting from **50a** (1.71 g, 5.13 mmol) and **52c** (1.4 g, 5.67 mmol) and following the procedure described for **8**, compound **15** was obtained as a white solid (0.100 g, 70%). Mp > 300 °C. ^{1}H NMR (500 MHz, CDCl$_3$) δ ppm 0.34−0.41 (m, 2H), 0.63−0.70 (m, 2H), 1.18−1.28 (m, 1H),

2.55 (s, 3H), 3.14 (d, J = 6.65 Hz, 2H), 6.73 (dd, J = 5.78, 2.31 Hz, 1H), 6.78 (d, J = 2.31 Hz, 1H), 6.91 (d, J = 7.22 Hz, 1H), 7.27−7.34 (m, 1H), 7.36−7.41 (m, 1H), 7.45 (dd, J = 10.69, 2.02 Hz, 1H), 8.01 (d, J = 6.94 Hz, 1H), 8.41 (d, J = 5.78 Hz, 1H). LC−MS m/z 409 [M + H]$^+$, t_R = 2.57 min.

8-Trifluoromethyl-3-cyclopropylmethyl-7-{4-[(2-methylpyridin-4-yl)oxy]-3-fluororophenyl}[1,2,4]triazolo[4,3-a]pyridine (16). Starting from **49a** (1.4 g, 5.08 mmol) and **52c** (1.84 g, 5.59 mmol) and following the procedure described for **8**, compound **16** was obtained as a white solid (0.233 g, 10%). Mp 194.6 °C. ^{1}H NMR (500 MHz, CDCl$_3$) δ ppm 0.34−0.44 (m, 2 H), 0.61−0.73 (m, 2H), 1.18−1.29 (m, 1H), 2.55 (s, 3H), 3.17 (d, J = 6.66 Hz, 2H), 6.70 (dd, J = 5.8, 2.6 Hz, 1H), 6.76 (d, J = 2.3 Hz, 1H), 6.83 (d, J = 7.2 Hz, 1H), 8.20 (br d, J = 8.4 Hz, 1H), 7.23−7.31 (m, 2H), 8.14 (d, J = 7.2 Hz, 1H), 8.41 (d, J = 5.8 Hz, 1H). LC−MS m/z 443 [M + H]$^+$, t_R = 2.70 min.

8-Chloro-3-cyclopropylmethyl-7-{4-[(2-ethylpyridin-4-yl)-oxy]-3-fluororophenyl}[1,2,4]triazolo[4,3-a]pyridine (17). Starting from **50a** (0.26 g, 0.78 mmol) and **52d** (0.293 g, 0.857 mmol) and following the procedure described for **8**, compound **17** was obtained as a white solid (0.316 g, 96%). Mp > 300 °C. ^{1}H NMR (500 MHz, CDCl$_3$) δ ppm 0.31−0.43 (m, 2H), 0.60−0.72 (m, 2H), 1.15−1.29 (m, 1H), 1.31 (t, J = 7.7 Hz, 3H), 2.82 (q, J = 7.6 Hz, 2H), 3.14 (d, J = 6.6 Hz, 2H), 6.72 (dd, J = 5.8, 2.3 Hz, 1H), 6.81 (d, J = 2.3 Hz, 1H), 6.91 (d, J = 6.9 Hz, 1H), 7.31 (t, J = 8.2 Hz, 1H), 7.35−7.42 (m, 1H), 7.45 (dd, J = 10.7, 2.0 Hz, 1H), 8.01 (d, J = 6.9 Hz, 1H), 8.44 (d, J = 5.8 Hz, 1H). LC−MS m/z 423 [M + H]$^+$, t_R = 2.04 min.

8-Trifluoromethyl-3-cyclopropylmethyl-7-{4-[(2,6-dimethyl-pyridin-4-yl)oxy]-3-fluororophenyl}[1,2,4]triazolo[4,3-a]-pyridine (18). Starting from **49a** (0.185 g, 0.67 mmol) and **52e** (0.3 g, 0.874 mmol) and following the procedure described for **8**, compound **18** was obtained as a white solid (0.100 g, 33%). Mp 232.5 °C. ^{1}H NMR (500 MHz, CDCl$_3$) δ ppm 0.24−0.50 (m, 2H), 0.55−0.79 (m, 2H), 1.05−1.39 (m, 1H), 2.50 (s, 6H), 3.17 (d, J = 6.70 Hz, 2H), 6.56 (s, 2H), 6.84 (d, J = 7.17 Hz, 1H), 7.16−7.21 (m, 1H), 7.22−7.29 (m, 2H), 8.14 (d, J = 7.17 Hz, 1 H). LC−MS m/z 457 [M + H]$^+$, t_R = 2.94 min.

8-Chloro-3-cyclopropylmethyl-7-{4-[(2-cyclopropylpyridin-4-yl)oxy]-3-fluororophenyl}[1,2,4]triazolo[4,3-a]pyridine (19). Starting from **50a** (0.103 g, 0.310 mmol) and **52f** (0.22 g, 0.310 mmol) and following the procedure described for **8**, compound **19** was obtained as a white solid (0.06 g, 45%). Mp > 300 °C. ^{1}H NMR (500 MHz, CDCl$_3$) δ ppm 0.38 (q, J = 5.11 Hz, 2H), 0.62−0.71 (m, 2H), 0.95−1.09 (m, 4H), 1.16−1.29 (m, 1H), 1.94−2.03 (m, 1H), 3.14 (d, J = 6.65 Hz, 2H), 6.66 (dd, J = 5.64, 2.46 Hz, 1H), 6.78 (d, J = 2.31 Hz, 1H), 6.90 (d, J = 6.94 Hz, 1H), 7.28−7.33 (m, 1H), 7.34−7.40 (m, 1H), 7.44 (dd, J = 10.69, 2.02 Hz, 1H), 8.00 (d, J = 6.94 Hz, 1H), 8.35 (d, J = 5.78 Hz, 1H). LC−MS m/z 435 [M + H]$^+$, t_R = 4.51 min.

8-Trifluoromethyl-3-cyclopropylmethyl-7-{4-[(2-cyclopro-pylpyridin-4-yl)oxy]-3-fluororophenyl}[1,2,4]triazolo[4,3-a]-pyridine (20). Starting from **49a** (0.2 g, 0.725 mmol) and **52f** (0.283 g, 0.798 mmol) and following the procedure described for **8**, compound **20** was obtained as a white solid (0.058 g, 17%). Mp 211.1 °C. ^{1}H NMR (500 MHz, CDCl$_3$) δ ppm 0.32−0.45 (m, 2H), 0.53−0.75 (m, 2H), 0.96−1.03 (m, 2H), 1.02−1.08 (m, 2H), 1.16−1.30 (m, 1H), 1.91−2.03 (m, 1H), 3.16 (d, J = 6.7 Hz, 2H), 6.63 (dd, J = 5.8, 2.3 Hz, 1H), 6.75 (d, J = 2.3 Hz, 1H), 6.83 (d, J = 7.2 Hz, 1H), 7.15−7.22 (m, 1H), 7.22−7.31 (m, 2H), 8.15 (d, J = 6.9 Hz, 1H), 8.35 (d, J = 5.5 Hz, 1H). LC−MS m/z 469 [M + H]$^+$, t_R = 3.31 min.

8-Chloro-3-(2,2,2-trifluoroethyl-7-{4-[(2,6-dimethylpyridin-3-yl)oxy]-3-fluorophenyl}[1,2,4]triazolo[4,3-a]pyridine (21). Starting from **56c** (0.2 g, 0.55 mmol) and **52a** (0.228 g, 0.664 mmol) and following the procedure described for **8**, compound **21** was obtained as a white solid (0.032 g, 13%). Mp 164.5 °C. ^{1}H NMR (500 MHz, CDCl$_3$) δ ppm 2.53 (s, 3H), 2.55 (s, 3H), 4.11 (q, J = 9.9 Hz, 2H), 6.93 (t, J = 8.3 Hz, 1H), 6.98 (d, J = 7.2 Hz, 1H), 7.02 (d, J = 8.3 Hz, 1H), 7.16 (d, J = 8.3 Hz, 1H), 7.23−7.28 (m, 1H), 7.42 (dd, J = 11.1, 2.1 Hz, 1H), 8.01 (d, J = 7.2 Hz, 1H). LC−MS m/z 451 [M + H]$^+$, t_R = 3.24 min.

8-Chloro-3-(ethoxymethyl-7-{4-[(2,6-dimethylpyridin-3-yl)-oxy]-3-fluorophenyl}[1,2,4]triazolo[4,3-a]pyridine (22). Starting from **50b** (0.4 g, 1.19 mmol) and **52a** (0.488 g, 1.42 mmol) and following the procedure described for **8**, compound **22** was obtained as a white solid (0.310 g, 61%). Mp 180.3 °C. ^{1}H NMR (500 MHz, CDCl$_3$)

δ ppm 1.23 (t, J = 6.94 Hz, 3H), 2.54 (s, 3 H), 2.55 (s, 3H), 3.58 (q, J = 6.94 Hz, 2H), 5.10 (s, 2H), 6.87−6.95 (m, 2H), 7.02 (d, J = 8.09 Hz, 1H), 7.16 (d, J = 8.09 Hz, 1H), 7.22−7.26 (m, 1H), 7.42 (dd, J = 11.27, 2.31 Hz, 1H), 8.25 (d, J = 7.22 Hz, 1H). LC−MS m/z 427 [M + H]$^+$, t_R = 2.77 min.

8-Trifluoromethyl-3-(ethoxymethyl-7-{4-[(2,6-dimethylpyridin-3-yl)oxy]-3-fluorophenyl}[1,2,4]triazolo[4,3-a]pyridine (23). Starting from **49b** (0.150 g, 0.536 mmol) and **52a** (0.239 g, 0.697 mmol) and following the procedure described for **8**, compound **23** was obtained as a white solid (0.150 g, 61%). Mp 142.2 °C. ^{1}H NMR (500 MHz, CDCl$_3$) δ ppm 1.23 (t, J = 7.08 Hz, 3H), 2.53 (s, 3H), 2.54 (s, 3H), 3.59 (q, J = 7.13 Hz, 2H), 5.12 (s, 2H), 6.82 (d, J = 7.22 Hz, 1H), 6.90 (t, J = 8.24 Hz, 1H), 7.01 (d, J = 8.38 Hz, 1H), 7.06 (d, J = 8.09 Hz, 1H), 7.14 (d, J = 8.38 Hz, 1H), 7.23 (dd, J = 10.69, 2.02 Hz, 1H), 8.40 (d, J = 6.94 Hz, 1H). LC−MS m/z 461 [M + H]$^+$, t_R = 2.89 min.

8-Chloro-3-cyclopropylmethyl-7-[3-fluoro-4-(isopropylamino)phenyl][1,2,4]triazolo[4,3-a]pyridine (24). Starting from **50a** (0.350 g, 1.049 mmol) and **52g** (0.381 g, 1.36 mmol) and following the procedure described for **8**, compound **24** was obtained as a white solid (0.097 g, 26%). Mp 196.4 °C. ^{1}H NMR (500 MHz, CDCl$_3$) δ ppm 0.35 (q, J = 5.20 Hz, 2H), 0.60−0.67 (m, 2H), 1.15−1.26 (m, 1H), 1.29 (d, J = 6.36 Hz, 6H), 3.10 (d, J = 6.65 Hz, H), 3.72 (dq, J = 13.19, 6.49 Hz, 1H), 3.98 (br d, J = 5.20 Hz, 1H), 6.70−6.81 (m, 1H), 6.87 (d, J = 6.94 Hz, 1H), 7.17−7.31 (m, 2H) 7.91 (d, J = 7.22 Hz, 1H). LC−MS m/z 359 [M + H]$^+$, t_R = 3.11 min.

8-Trifluoromethyl-3-cyclopropylmethyl-7-[3-fluoro-4-(isopropylamino)phenyl][1,2,4]triazolo[4,3-a]pyridine (25). Starting from **49a** (0.350 g, 1.27 mmol) and **52g** (0.461 g, 1.65 mmol) and following the procedure described for **8**, compound **25** was obtained as a white solid (0.250 g, 50%). Mp 196.9 °C. ^{1}H NMR (500 MHz, CDCl$_3$) δ ppm 0.28−0.42 (m, 2H), 0.57−0.71 (m, 2H), 1.12−1.26 (m, 1H), 1.29 (d, J = 6.4 Hz, 6H), 3.12 (d, J = 6.6 Hz, 2H), 3.64−3.77 (m, 1H), 3.96 (d, J = 4.9 Hz, 1H), 6.74 (t, J = 8.4 Hz, 1H), 6.80 (d, J = 7.2 Hz, 1H), 7.02 (d, J = 10.1 Hz, 2H), 8.04 (d, J = 6.9 Hz, 1H). LC−MS m/z 393 [M + H]$^+$, t_R = 3.33 min.

8-Trifluoromethyl-3-cyclopropylmethyl-7-[3-chloro-4-(isopropylamino)phenyl][1,2,4]triazolo[4,3-a]pyridine (26). Starting from **49a** (0.350 g, 1.27 mmol) and **52h** (0.488 g, 1.65 mmol) and following the procedure described for **8**, compound **26** was obtained as a white solid (0.250 g, 50%). Mp 230 °C. ^{1}H NMR (500 MHz, CDCl$_3$) δ ppm 0.29−0.42 (m, 2H), 0.55−0.71 (m, 2H), 1.11−1.27 (m, 1H), 1.31 (d, J = 6.36 Hz, 6H), 3.13 (d, J = 6.65 Hz, 2H), 3.73 (dq, J = 13.11, 6.51 Hz, 1H), 4.38 (br d, J = 7.51 Hz, 1H), 6.71 (d, J = 8.67 Hz, 1H), 6.79 (d, J = 7.22 Hz, 1H), 7.16 (dd, J = 8.38, 1.44 Hz, 1H), 7.30 (d, J = 2.02 Hz, 1H), 8.03 (d, J = 6.94 Hz, 1H). LC−MS m/z 409 [M + H]$^+$, t_R = 3.71 min.

8-Chloro-3-cyclopropylmethyl-7-[3-fluoro-4-(cyclopropylamino)phenyl][1,2,4]triazolo[4,3-a]pyridine (27). Starting from **50a** (0.30 g, 0.9 mmol) and **52i** (0.3 g, 1.08 mmol) and following the procedure described for **8**, compound **27** was obtained as a white solid (0.147 g, 46%). ^{1}H NMR (500 MHz, CDCl$_3$) δ ppm 0.28−0.40 (m, 2H), 0.57−0.69 (m, 4H), 0.78−0.87 (m, 2H), 1.15−1.28 (m, 1H), 2.45−2.56 (m, 1H), 3.11 (d, J = 6.65 Hz, 2H), 4.60 (br s, 1H), 6.88 (d, J = 7.22 Hz, 1H), 7.13−7.20 (m, 1H), 7.21−7.31 (m, 2H), 7.92 (d, J = 6.94 Hz, 1H). LC−MS m/z 357 [M + H]$^+$, t_R = 3.30 min.

8-Trifluoromethyl-3-cyclopropylmethyl-7-[3-fluoro-4-(cyclopropylamino)phenyl][1,2,4]triazolo[4,3-a]pyridine (28). Starting from **49a** (0.20 g, 0.73 mmol) and **52i** (0.221 g, 0.8 mmol) and following the procedure described for **8**, compound **28** was obtained as a white solid (0.169 g, 60%). Mp > 300 °C. ^{1}H NMR (400 MHz, CDCl$_3$) δ ppm 0.28−0.43 (m, 2H), 0.51−0.72 (m, 4H), 0.75−0.91 (m, 2H), 1.12−1.31 (m, 1H), 2.50 (tt, J = 6.56, 3.27 Hz, 1H), 3.13 (d, J = 6.70 Hz, 2H), 4.58 (br s, 1H), 6.80 (d, J = 6.94 Hz, 1H), 6.98−7.09 (m, 2H), 7.10−7.18 (m, 1H), 8.05 (d, J = 7.17 Hz, 1H). LC−MS m/z 391 [M + H]$^+$, t_R = 3.18 min.

8-Trifluoromethyl-3-cyclopropylmethyl-7-[3-chloro-4-(cyclopropylamino)phenyl][1,2,4]triazolo[4,3-a]pyridine (29). Starting from **49a** (0.20 g, 0.73 mmol) and **52j** (0.34 g, 0.8 mmol) and following the procedure described for **8**, compound **29** was obtained as a white solid (0.109 g, 37%). ^{1}H NMR (400 MHz, CDCl$_3$) δ ppm 0.31−0.40 (m, 2H), 0.59−0.69 (m, 4H), 0.81−0.89 (m, 2H), 1.15−1.27

(m, 1H), 2.46−2.56 (m, 1H), 3.13 (d, J = 6.70 Hz, 2H), 4.93 (s, 1H), 6.80 (d, J = 7.17 Hz, 1H), 7.11−7.16 (m, 1H), 7.17−7.23 (m, 1H), 7.28 (d, J = 1.85 Hz, 1H), 8.05 (d, J = 7.17 Hz, 1H). LC−MS m/z 407 [M + H]$^+$, t_R = 3.48 min.

8-Chloro-3-cyclopropylmethyl-7-[3-chloro-4-(cyclopropylamino)phenyl][1,2,4]triazolo[4,3-a]pyridine (30). Starting from **50a** (0.30 g, 0.9 mmol) and **52j** (0.32 g, 1.08 mmol) and following the procedure described for **8**, compound **30** was obtained as a white solid (0.147 g, 46%). Mp > 300 °C. ^{1}H NMR (500 MHz, CDCl$_3$) δ ppm 0.29−0.42 (m, 2H), 0.57−0.70 (m, 4H), 0.78−0.92 (m, 2H), 1.15−1.27 (m, 1H), 2.49−2.56 (m, 1H), 3.11 (d, J = 6.7 Hz, 2H), 4.60 (br s, 1H), 6.87 (d, J = 6.9 Hz, 1H), 7.18 (d, J = 8.3 Hz, 1H), 7.42 dd, J = 8.3, 2.1 Hz, 1H), 7.47 (d, J = 1.8 Hz, 1H), 7.92 (d, J = 7.2 Hz, 1H). LC−MS m/z 373 [M + H]$^+$, t_R = 3.83 min.

8-Trifluoromethyl-3-cyclopropylmethyl-7-{4-[(2-methoxypyridin-5-yl)methoxy]-3-fluorophenyl}[1,2,4]triazolo[4,3-a]pyridine (31). Starting from **49a** (0.3 g, 1.088 mmol) and **52k** (0.721 g, 1.306 mmol) and following the procedure described for **8**, compound **31** was obtained as a white solid (0.198 g, 38%). Mp 148.5 °C. ^{1}H NMR (400 MHz, CDCl$_3$) δ ppm 0.37 (q, J = 5.09 Hz, 2H), 0.56−0.74 (m, 2H), 1.09−1.32 (m, 1H), 3.14 (d, J = 6.70 Hz, 2H), 3.96 (s, 3H), 5.12 (s, 2H), 6.79 (dd, J = 13.87, 7.63 Hz, 2H), 7.00−7.19 (m, 3H), 7.71 (dd, J = 8.55, 2.54 Hz, 1H) 8.09 (d, J = 7.17 Hz, 1H), 8.24 (d, J = 2.31 Hz, 1H). LC−MS m/z 473 [M + H]$^+$, t_R = 2.79 min.

8-Trifluoromethyl-3-cyclopropylmethyl-7-{4-[(2-methoxypyridin-5-yl)methoxy]phenyl}[1,2,4]triazolo[4,3-a]pyridine (32). Starting from **49a** (0.315 g, 1.15 mmol) and **52l** (0.430 g, 1.26 mmol) and following the procedure described for **8**, compound **32** was obtained as a white solid (0.286 g, 60%). Mp 159.1 °C. ^{1}H NMR (400 MHz, CDCl$_3$) δ ppm 0.29−0.45 (m, 2H), 0.55−0.72 (m, 2H), 1.10−1.33 (m, 1H), 3.14 (d, J = 6.70 Hz, 2H), 3.96 (s, 3H), 5.04 (s, 2H), 6.67−6.87 (m, 2H), 7.00−7.12 (m, 2H), 7.32 (d, J = 8.55 Hz, 2H), 7.70 (dd, J = 8.55, 2.31 Hz, 1H), 8.08 (d, J = 7.17 Hz, 1H), 8.25 (d, J = 2.31 Hz, 1H). LC−MS m/z 455 [M + H]$^+$, t_R = 3.73 min.

8-Trifluoromethyl-3-cyclopropylmethyl-7-{4-[(2-methoxypyridin-5-yl)methylamino]-3-fluorophenyl}[1,2,4]triazolo[4,3-a]pyridine (33). Starting from **49a** (0.530 g, 1.92 mmol) and **52m** (0.758 g, 2.11 mmol) and following the procedure described for **8**, compound **33** was obtained as a white solid (0.460 g, 51%). Mp 160.4 °C. ^{1}H NMR (400 MHz, CDCl$_3$) δ ppm 0.30−0.47 (m, 2H), 0.59−0.71 (m, 2H), 1.15−1.27 (m, 1H), 3.13 (d, J = 6.70 Hz, 2H), 3.95 (s, 3H), 4.36 (d, J = 4.86 Hz, 2H), 4.44 (br s, 1H), 6.69−6.83 (m, 3H), 6.95−7.12 (m, 2H), 7.62 (dd, J = 8.44, 2.43 Hz, 1H), 8.05 (d, J = 7.17 Hz, 1H), 8.19 (d, J = 2.54 Hz, 1H). LC−MS m/z 472 [M + H]$^+$, t_R = 2.67 min.

8-Trifluoromethyl-3-cyclopropylmethyl-7-{4-[(2-methoxypyridin-5-yl)methylamino]-3-phenyl}[1,2,4]triazolo[4,3-a]pyridine (34). Starting from **49a** (0.150 g, 0.544 mmol) and **52n** (0.204 g, 0.6 mmol) and following the procedure described for **8**, compound **34** was obtained as a white solid (0.115 g, 46%). Mp 127.5 °C. ^{1}H NMR (500 MHz, CDCl$_3$) δ ppm 0.29−0.42 (m, 2H), 0.60−0.68 (m, 2H), 1.17−1.24 (m, 1H), 3.12 (d, J = 6.94 Hz, 2H), 3.95 (s, 3H), 4.20 (br s, 1H), 4.32 (d, J = 4.91 Hz, 2H), 6.70 (d, J = 8.38 Hz, 2H), 6.76 (d, J = 8.38 Hz, 1H), 6.80 (d, J = 6.94 Hz, 1H), 7.21 (d, J = 8.67 Hz, 2H), 7.61 (dd, J = 8.53, 2.46 Hz, 1H), 8.03 (d, J = 7.22 Hz, 1H), 8.18 (d, J = 2.31 Hz, 1H). LC−MS m/z 454 [M + H]$^+$, t_R = 2.05 min.

8-Chloro-3-cyclopropylmethyl-7-{4-[(2-methoxypyridin-5-yl)methylamino]-3-phenyl}[1,2,4]triazolo[4,3-a]pyridine (35). Starting from **50a** (0.150 g, 0.45 mmol) and **52n** (0.168 g, 0.494 mmol) and following the procedure described for **8**, compound **35** was obtained as a white solid (0.098 g, 51%). Mp 158.1 °C. ^{1}H NMR (400 MHz, CDCl$_3$) δ ppm 0.30−0.40 (m, 2H), 0.57−0.70 (m, 2H), 1.13−1.39 (m, 1H), 3.10 (d, J = 6.70 Hz, 2H), 3.95 (s, 3H), 4.33 (s, 3H), 6.69−6.79 (m, 3H), 6.89 (d, J = 7.17 Hz, 1H), 7.38−7.46 (m, 2H), 7.62 (dd, J = 8.55, 2.54 Hz, 1H), 7.91 (d, J = 7.17 Hz, 1H), 8.19 (d, J = 2.08 Hz, 1H). LC−MS m/z 420 [M + H]$^+$, t_R = 1.93 min.

8-Chloro-3-cyclopropylmethyl-7-[3-chloro-4-(tetrahydropyran-4-yloxy)phenyl][1,2,4]triazolo[4,3-a]pyridine (36). Starting from **50a** (0.20 g, 0.6 mmol) and **52o** (0.243 g, 0.72 mmol) and following the procedure described for **8**, compound **36** was obtained as a white solid (0.160 g, 64%). Mp 189.1 °C. ^{1}H NMR (400 MHz, CDCl$_3$) δ ppm 0.30−0.43 (m, 2H), 0.56−0.73 (m, 2H), 1.15−1.30 (m, 1H),

1.92 (ddt, J = 17.05, 7.28, 3.55, 3.55 Hz, 2H), 2.02−2.17 (m, 2H), 3.12 (d, J = 6.70 Hz, 2H), 3.65 (ddd, J = 11.44, 7.40, 3.58 Hz, 2H), 4.05 (ddd, J = 11.44, 7.40, 3.58 Hz, 2H), 4.66 (tt, J = 7.11, 3.64 Hz, 1H), 6.86 (d, J = 6.94 Hz, 1H), 7.06 (d, J = 8.55 Hz, 1H), 7.43 (dd, J = 8.55, 2.31 Hz, 1H), 7.58 (d, J = 2.31 Hz, 1H), 7.96 (d, J = 7.17 Hz, 1H). LC−MS m/z 418 [M + H]$^+$, t_R = 3.25 min.

8-Trifluoromethyl-3-cyclopropylmethyl-7-[3-chloro-4-(tetrahydropyran-4-yloxy)phenyl][1,2,4]triazolo[4,3-a]pyridine (37). Starting from **49a** (0.09 g, 0.33 mmol) and **52o** (0.138 g, 0.41 mmol) and following the procedure described for **8**, compound **37** was obtained as a white solid (0.083 g, 56%). Mp 176.9 °C. ^{1}H NMR (400 MHz, CDCl$_3$) δ ppm 0.30−0.43 (m, 2H), 0.58−0.73 (m, 2H), 1.16−1.28 (m, 1H), 1.86−1.97 (m, 2H), 2.02−2.12 (m, 2H), 3.14 (d, J = 6.70 Hz, H), 3.59−3.69 (m, 2H), 4−4.09 (m, 2H), 4.61−4.68 (m, 2H), 6.78 (d, J = 7.2 Hz, 1H), 7.02 (d, J = 8.6 Hz, 1H), 7.20 (dd, J = 8.6, 2.1 Hz, 1H), 7.41 (d, J = 2.1 Hz, 1H), 8.09 (d, J = 7.2 Hz, 1H). LC−MS m/z 452 [M + H]$^+$, t_R = 3.33 min.

8-Chloro-3-cyclopropylmethyl-7-[3-chloro-4-(tetrahydropyran-4-ylamino)phenyl][1,2,4]triazolo[4,3-a]pyridine (38). Starting from **50a** (0.20 g, 0.6 mmol) and **52p** (0.242 g, 0.72 mmol) and following the procedure described for **8**, compound **38** was obtained as a white solid (0.160 g, 64%). Mp 221.3 °C. ^{1}H NMR (500 MHz, CDCl$_3$) δ ppm 0.28−0.41 (m, 2H), 0.56−0.71 (m, 2H), 1.13−1.29 (m, 1H), 1.45−1.71 (m, 2H), 2.10 (br d, J = 13.29 Hz, 2H), 3.11 (d, J = 6.65 Hz, 2H), 3.52−3.60 (m, 2H), 3.62 (br dd, J = 6.94, 3.18 Hz, 1H), 4.05 (dt, J = 11.78, 3.65 Hz, 2H), 4.49 (br d, J = 7.80 Hz, 1H), 6.78 (d, J = 8.38 Hz, 1H), 6.86 (d, J = 7.22 Hz, 1H), 7.39 (dd, J = 8.53, 2.17 Hz, 1H), 7.51 (d, J = 2.31 Hz, 1H), 7.92 (d, J = 7.22 Hz, 1H). LC−MS m/z 417 [M + H]$^+$, t_R = 4.08 min.

8-Trifluoromethyl-3-cyclopropylmethyl-7-[3-chloro-4-(tetrahydropyran-4-ylamino)phenyl][1,2,4]triazolo[4,3-a]pyridine (39). Starting from **49a** (0.07 g, 0.25 mmol) and **52p** (0.107 g, 0.32 mmol) and following the procedure described for **8**, compound **39** was obtained as a white solid (0.045 g, 39%). Mp 198.4 °C. ^{1}H NMR (400 MHz, CDCl$_3$) δ ppm 0.31−0.42 (m, 2H), 0.58−0.71 (m, 2H), 1.16−1.27 (m, 1H), 1.55−1.68 (m, 2H), 2.09 (br d, J = 12.7 Hz, 2H), 3.13 (d, J = 6.7 Hz, 2H), 3.56 (td, J = 11.8, 2.3 Hz, 1H), 3.56−3.67 (m, 1H), 4.05 (dt, J = 11.7, 3.7 Hz, 2H), 4.47 (d, J = 7.6 Hz, 1H), 6.74 (d, J = 8.6 Hz, 1H), 6.78 (d, J = 7.2 Hz, 1H), 7.16 (dd, J = 8.3, 1.8 Hz, 1H), 7.32 (d, J = 2.1 Hz, 1H), 8.05 (d, J = 7.2 Hz, 1H). LC−MS m/z 451 [M + H]$^+$, t_R = 3.29 min.

8-Trifluoromethyl-3-cyclopropylmethyl-7-[3-chloro-4-(tetrahydropyran-4-ylaminomethyl)phenyl][1,2,4]triazolo[4,3-a]pyridine (40). Starting from **49a** (0.2 g, 0.73 mmol) and **52q** (0.306 g, 0.87 mmol) and following the procedure described for **8**, compound **40** was obtained as a white solid (0.060 g, 18%). ^{1}H NMR (400 MHz, CDCl$_3$) δ ppm 0.37 (q, J = 5.09 Hz, 2H), 0.59−0.74 (m, 2H), 1.10−1.32 (m, 2H), 1.41−1.73 (m, 2H), 1.92 (br dd, J = 12.60, 1.73 Hz, 2H), 2.69−2.86 (m, 1H), 3.15 (d, J = 6.70 Hz, 2H), 3.34−3.49 (m, 2H), 3.97−4.01 (m, 3H), 4.01−4.04 (m, 1H), 6.76 (d, J = 7.17 Hz, 1H), 7.22−7.28 (m, 1H), 7.37 (d, J = 1.62 Hz, 1H), 7.56 (d, J = 7.86 Hz, 1H), 8.10 (d, J = 7.17 Hz, 1H). LC−MS m/z 465 [M + H]$^+$, t_R = 2.09 min.

trans-8-Chloro-3-cyclopropylmethyl-7-[3-chloro-4-(4-hydroxycyclohexylamino)phenyl][1,2,4]triazolo[4,3-a]pyridine (41). Starting from **50a** (0.13 g, 0.388 mmol) and **52r** (0.15 g, 0.43 mmol) and following the procedure described for **8**, compound **41** was obtained as a white solid (0.087 g, 52%). Mp 270.9 °C. ^{1}H NMR (400 MHz, CDCl$_3$) δ ppm 0.29−0.42 (m, 2H), 0.56−0.71 (m, 2H), 1.17−1.25 (m, 1H), 1.47 (br s, 1H), 1.73−1.8 (m, 4H), 1.80−1.91 (m, 4H), 3.11 (d, J = 6.7 Hz, 2H), 3.46−3.57 (m, 1H), 3.98 (br s, 1H), 4.60 (br d, J = 7.6 Hz, 1H), 6.76 (d, J = 8.8 Hz, 1H), 6.87 (d, J = 7.2 Hz, 1H), 7.39 (dd, J = 8.3, 2.3 Hz, 1H), 7.49 (d, J = 2.1 Hz, 1H), 7.91 (d, J = 7.2 Hz, 1H). LC−MS m/z 431 [M + H]$^+$, t_R = 3.49 min.

trans-8-Trifluoromethyl-3-cyclopropylmethyl-7-[3-chloro-4-(4-hydroxycyclohexylamino)phenyl][1,2,4]triazolo[4,3-a]pyridine (42). Starting from **49a** (0.3 g, 1.088 mmol) and **52r** (0.459 g, 1.306 mmol) and following the procedure described for **8**, compound **42** was obtained as a white solid (0.209 g, 41%). Mp 290.7 °C. ^{1}H NMR (400 MHz, CDCl$_3$) δ ppm 0.3−0.43 (m, 2H), 0.58−0.71 (m, 2H), 1.16−1.25 (m, 1H), 1.29−1.42 (m, 2H), 1.42−1.53 (m, 3H), 2.03−2.12 (m, 2H), 2.20 (br d, J = 12.0 Hz, 2H), 3.13 (d, J = 6.7 Hz, 2H), 3.32−

3.43 (m, 1H), 3.70−3.80 (m, 1H), 4.39 (d, *J* = 7.6 Hz, 1H), 6.72 (d, *J* = 8.6 Hz, 1H), 6.79 (d, *J* = 7.2 Hz, 1H), 7.16 (dd, *J* = 8.6, 2.1 Hz, 1H), 7.30 (d, *J* = 2.1 Hz, 1H), 8.04 (d, *J* = 7.2 Hz, 1H). LC−MS *m/z* 465 [M + H]⁺, *t*_R = 2.50 min.

cis-8-Chloro-3-cyclopropylmethyl-7-[3-chloro-4-(4-hydroxy-cyclohexylamino)phenyl][1,2,4]triazolo[4,3-a]pyridine (43). Starting from **50a** (0.13 g, 0.388 mmol) and **52s** (0.15 g, 0.43 mmol) and following the procedure described for **8**, compound **43** was obtained as a white solid (0.060 g, 36%). Mp 273.7 °C. ¹H NMR (400 MHz, CDCl₃) δ ppm 0.27−0.43 (m, 2H) 0.57−0.70 (m, 2H), 1.02−1.32 (m, 2H), 1.68−1.98 (m, 8H), 3.11 (d, *J* = 6.70 Hz, 2H), 3.44−3.62 (m, 1H), 3.98 (br s, 1H), 4.60 (br d, *J* = 7.63 Hz, 1H), 6.76 (d, *J* = 8.79 Hz, 1H), 6.87 (d, *J* = 7.17 Hz, 1H), 7.39 (dd, *J* = 8.44, 2.20 Hz, 1H), 7.49 (d, *J* = 2.08 Hz, 1H), 7.91 (d, *J* = 7.17 Hz, 1H). LC−MS *m/z* 431 [M + H]⁺, *t*_R = 3.08 min.

cis-8-Trifluoromethyl-3-cyclopropylmethyl-7-[3-chloro-4-(4-hydroxy-4-cyclopropylcyclohexylamino)phenyl][1,2,4]-triazolo[4,3-a]pyridine (44). Starting from **49a** (0.143 g, 0.52 mmol) and **52t** (0.235 g, 0.6 mmol) and following the procedure described for **8**, compound **44** was obtained as a white solid (0.047 g, 18%). Mp > 300 °C. ¹H NMR (500 MHz, CDCl₃) δ ppm 0.04−0.16 (m, 2H), 0.18−0.33 (m, 5H), 0.34−0.43 (m, 2H), 0.60 (tt, *J* = 8.31, 5.56 Hz, 1H), 0.80−1.00 (m, 1H), 1.11−1.25 (m, 2H), 1.31−1.56 (m, 4H), 1.63−1.79 (m, 2H), 2.49 (d, *J* = 6.65 Hz, 2H), 2.97 (tdt, *J* = 11.13, 11.13, 7.37, 3.97, 3.97 Hz, 1H), 4.45 (d, *J* = 7.51 Hz, 1H), 5.95 (d, *J* = 7.22 Hz, 1H), 6.53 (d, *J* = 8.67 Hz, 1H), 6.73 (d, *J* = 7.22 Hz, 1H), 7.16 (s, 1H) 7.28 (d, *J* = 2.02 Hz, 1H). LC−MS *m/z* 465 [M + H]⁺, *t*_R = 3.49 min.

trans-8-Chloro-3-(2,2,2-trifluoroethyl)-7-[3-chloro-4-(4-hydroxycyclohexylamino)phenyl][1,2,4]triazolo[4,3-a]pyridine (45). Starting from **56c** (0.11 g, 0.304 mmol) and **52r** (0.128 g, 0.365 mmol) and following the procedure described for **8**, compound **45** was obtained as a white solid (0.054 g, 39%). Mp > 300 °C. ¹H NMR (400 MHz, CDCl₃) δ ppm 1.28−1.52 (m, 5H), 2.08 (br d, *J* = 10.63 Hz, 2H), 2.20 (br d, *J* = 12.02 Hz, 2H), 3.26−3.46 (m, 1H), 3.62−3.85 (m, 1H), 4.08 (q, *J* = 9.71 Hz, 2H), 4.44 (d, *J* = 7.63 Hz, 1H), 6.77 (d, *J* = 8.55 Hz, 1H), 6.97 (d, *J* = 7.17 Hz, 1H), 7.39 (dd, *J* = 8.55, 2.08 Hz, 1H), 7.50 (d, *J* = 2.08 Hz, 1H), 7.94 (d, *J* = 7.17 Hz, 1H). LC−MS *m/z* 459 [M + H]⁺, *t*_R = 3.23 min.

trans-8-Trifluoromethyl-3-cyclopropylmethyl-7-[3-chloro-4-(4-hydroxycyclohexyloxy)phenyl][1,2,4]triazolo[4,3-a]pyridine (46). Starting from **49a** (0.119 g, 0.432 mmol) and **52u** (0.183g, 0.518 mmol) and following the procedure described for **8**, compound **46** was obtained as a white solid (0.022 g, 27%). ¹H NMR (400 MHz, CDCl₃) δ ppm 0.31−0.41 (m, 2H), 0.61−0.71 (m, 2H), 1.09−1.32 (m, 2H), 1.42−1.56 (m, 2H), 1.67−1.80 (m, 2H), 2.05−2.23 (m, 4H), 3.14 (d, *J* = 6.70 Hz, 2H), 3.83−3.96 (m, 1H), 4.36−4.49 (m, 1H), 6.78 (d, *J* = 7.17 Hz, 1H), 7.02 (d, *J* = 8.79 Hz, 1H), 7.20 (dd, *J* = 8.44, 2.20 Hz, 1H), 7.39 (d, *J* = 2.31 Hz, 1H), 8.09 (d, *J* = 7.17 Hz, 1H). LC−MS *m/z* 466 [M + H]⁺, *t*_R = 2.96 min.

trans-8-Chloro-3-(2,2,2-trifluoroethyl)-7-[3-chloro-4-(4-hydroxycyclohexyloxy)phenyl][1,2,4]triazolo[4,3-a]pyridine (47). Starting from **56c** (0.190 g, 0.526 mmol) and **52u** (0.222 g, 0.631 mmol) and following the procedure described for **8**, compound **47** was obtained as a white solid (0.065 g, 27%). Mp > 300 °C. ¹H NMR (500 MHz, CDCl₃) δ ppm 1.42 (d, *J* = 3.76 Hz, 1H), 1.46−1.55 (m, 2H), 1.68−1.79 (m, 2H), 2.10 (td, *J* = 7.73, 3.61 Hz, 2H), 2.18 (td, *J* = 7.66, 3.47 Hz, 2H), 3.91 (td, *J* = 8.09, 4.05 Hz, 1H), 4.10 (q, *J* = 9.73 Hz, 2H), 4.46 (tt, *J* = 8.06, 3.79 Hz, 1H), 6.97 (d, *J* = 7.22 Hz, 1H), 7.08 (d, *J* = 8.38 Hz, 1H), 7.42 (dd, *J* = 8.53, 2.17 Hz, 1H), 7.57 (d, *J* = 2.31 Hz, 1H), 7.98 (d, *J* = 7.22 Hz, 1H). LC−MS *m/z* 460 [M + H]⁺, *t*_R = 3.23 min.

cis-8-Chloro-3-(2,2,2-trifluoroethyl)-7-[3-chloro-4-(4-hydroxycyclohexyloxy)phenyl][1,2,4]triazolo[4,3-a]pyridine (48). Starting from **56c** (0.150 g, 0.415 mmol) and **52v** (0.176g, 0.498 mmol) and following the procedure described for **8**, compound **48** was obtained as a white solid (0.044 g, 23%). Mp 196.7 °C. ¹H NMR (400 MHz, CDCl₃) δ ppm 1.39−1.48 (m, 1H), 1.66−1.93 (m, 6H), 2.06−2.21 (m, 2H), 3.81 (tq, *J* = 8.44, 4.24 Hz, 1H), 4.10 (q, *J* = 9.71 Hz, 2H), 4.56 (tt, *J* = 5.20, 2.77 Hz, 1H), 6.98 (d, *J* = 7.17 Hz, 1H), 7.06 (d, *J* = 8.55 Hz, 1H), 7.43 (dd, *J* = 8.55, 2.31 Hz, 1H), 7.57 (d, *J* = 2.31 Hz, 1H), 7.99 (d, *J* = 7.17 Hz, 1H). LC−MS *m/z* 460 [M + H]⁺, *t*_R = 3.14 min.

8-Trifluoromethyl-3-(ethoxymethyl)-7-[3-chloro-1,2,4-triazolo[4,3-a]pyridine (49b). Mp 104 °C. ¹H NMR (400 MHz, CDCl₃) δ ppm 1.22 (t, *J* = 6.94 Hz, 3 H), 3.57 (q, *J* = 6.94 Hz, 2 H), 5.08 (s, 2 H), 6.95 (d, *J* = 7.22 Hz, 1 H), 8.35 (d, *J* = 7.51 Hz, 1 H). LC−MS *m/z* 280 [M + H]⁺, *t*_R = 1.32 min.

Biology. *Membrane Preparation.* CHO-K1 cells stably expressing the wild-type hmGlu₂ receptor (CHO-K1_hmGlu₂) were grown in DMEM medium supplemented with 10% (v/v) fetal calf serum, 200 IU/mL penicillin, 200 μg/mL streptomycin, 30.5 μg/mL L-proline, and 400 μg/mL G418 at 37 °C and 5% CO₂. Sodium butyrate (final concentration 5 mM) was added to the plates when cells growth reached 70% confluency.[63] 24 h later, cells were detached from the plates by scraping them into 5 mL of PBS and were centrifuged for 5 min at 1500 rpm. Pellets were resuspended into ice-cold Tris buffer (50 mM Tris-HCl, pH 7.4) and homogenized using an Ultra Turrax homogenizer (IKA Werke GmbH & Co.KG, Staufen, Germany). An Optima LE 80 K ultracentrifuge (Beckman Coulter, Fullerton, CA) at 31 000 rpm was used for separation of membranes and the cytosolic fraction at 4 °C for 20 min. Pellets were resuspended in 10 mL of Tris buffer, and the centrifugation and homogenization steps were repeated. Remaining pellets were suspended into assay buffer (50 mM Tris-HCl, pH 7.4, 2 mM CaCl₂, 10 mM MgCl₂), and the homogenization step was repeated. Aliquots were stored at −80 °C. BCA protein determination was used to determine the membrane protein concentrations.

[³⁵S]GTPγS Binding Assay. [³⁵S]GTPγS binding experiments were performed as previously described.[12]

Radioligand Binding Assays. After thawing, membranes were homogenized by an Ultra Turrax homogenizer. **4** (10 μM) was used to determine nonspecific binding. DMSO concentrations were ≤0.25%. For all experiments, radioligand concentrations were such that <10% of the amount added was receptor-bound to avoid ligand depletion.

For displacement assays, membrane protein aliquots (30 μg) were incubated with 6 nM [³H]-**7** and 10 concentrations of competing ligand diluted by an HP D300 digital dispenser (Tecan, Giessen, The Netherlands) in assay buffer to a total volume of 100 μL. After 60 min at 15 °C, incubation was terminated by rapid filtration over GF/C filter plates (PerkinElmer, Groningen, The Netherlands) on a PerkinElmer Filtermate harvester. Filter plates were washed 10 times with ice-cold wash buffer (50 mM Tris-HCl, pH 7.4), and filter-bound radioactivity was determined in a Microbeta 2450² microplate counter (PerkinElmer).

For association, dissociation, and competition association experiments a scintillation proximity assay (SPA) was developed and used. Membrane protein (20 μg) and prewetted wheat-germ agglutinin coated SPA beads (0.2 mg; RPNQ0001, PerkinElmer) were precoupled in assay buffer while gently shaking at room temperature for 30 min. Then, this membrane bead mixture was added to an Isoplate-96 (PerkinElmer) together with 6 nM [³H]-**7** and competing ligand in case of competition association. After addition, the plate was rapidly placed in a Microbeta 2450² microplate counter. Plates were recorded for 120 min measuring every 30 s at ambient temperature of 28 °C. Binding values were determined in corrected counts per minute (CCPM). For dissociation assays, radioligand dissociation was initiated after 60 min of incubation by addition of 5 μL of **4** (final concentration: 10 μM). Subsequently, plates were recorded for 120 min being measured every 30 s.

Label-Free Whole-Cell Assays. Label-free whole-cell assays were performed using the xCELLigence real-time cell analyzer (RTCA DP) system as described previously.[58,64] Baseline impedance was measured using 45 μL of culture medium (as described under membrane preparation) per well in 16-well E-plates (Westburg, Leusden, The Netherlands). 40 000 cells per well were added in a volume of 50 μL. After resting for 30 min at room temperature, E-plates were placed in the recording station within a humidified 37 °C, 5% CO₂ incubator. Impedance (represented in the arbitrary unit cell index) was measured every 15 min overnight. After 18 h, cells were stimulated with the indicated concentration of compound. Impedance was measured every 15 s for 20 min, then 5 min intervals were used for the next 40 min, followed by 15 min intervals thereafter. For washing experiments, cells were stimulated with an EC₈₀ equivalent concentration of compound in

a volume of 5 μL. Wells were washed after 5 min by aspiration of the medium, addition of 100 μL of fresh medium, which was subsequently aspirated and replaced by another 100 μL of fresh medium. This washing step was chosen such that it was just before the maximum cell index level. In control wells, medium was pipetted up and down in order to induce similar mechanical cell stress.

Data Analysis. Data analyses were performed using Prism 6.04 (GraphPad software, San Diego, CA, USA). pIC_{50} values were acquired using nonlinear regression curve fitting into a sigmoidal concentration–response curve using the equation: $Y = \text{Bottom} + (\text{Top} - \text{Bottom})/(1 + 10^{(X - \log IC_{50})})$. $(p)K_i$ values were acquired from $(p)IC_{50}$ values using the Cheng–Prusoff equation.[65] Dissociation rate constants k_{off} were determined using an exponential decay analysis of radioligand binding. Association rate constants k_{on} were determined using the equation $k_{on} = (k_{obs} - k_{off})/[L]$, in which L is the concentration of radioligand used for association experiments and k_{obs} was determined using exponential association analysis.

Association and dissociation rate constants for unlabeled $mGlu_2$ PAMs were determined by nonlinear regression analysis of competition association data as described by Motulsky and Mahan.[40]

$$K_A = k_1[L](10^{-9}) + k_2$$

$$K_B = k_3[I](10^{-9}) + k_4$$

$$S = \sqrt{(K_A - K_B)^2 + 4k_1 k_3 LI(10^{-18})}$$

$$K_F = 0.5(K_A + K_B + S)$$

$$K_S = 0.5(K_A + K_B - S)$$

$$Q = \frac{B_{max} k_1 L(10^{-9})}{K_F - K_S}$$

$$Y = Q\left(\frac{k_4(K_F - K_S)}{K_F K_S} + \frac{k_4 - K_F}{K_F}e^{(-K_F X)} - \frac{k_4 - K_S}{K_S}e^{(-K_S X)}\right)$$

Experimental data are reported as k_{on} and k_{off}, and the corresponding conversion of k_{off} to residence time (RT) is performed to be consistent with current state of the art.[24]

Data shown are the mean ± SEM of at least three individual experiments performed in duplicate unless stated otherwise. Statistical analysis was performed if indicated, using a two-tailed unpaired Student's t test. Observed differences with p-values of <0.05 were considered statistically significant. clogP values were calculated using ChemDraw Professional version 15.0.0.106 (PerkinElmer).

ASSOCIATED CONTENT

Supporting Information

The Supporting Information is available free of charge on the ACS Publications website at DOI: 10.1021/acs.jmedchem.7b00669.

> Additional correlation plots, $mGlu_2$ PAM response on CHO-K1 WT cells, effect of PAM treatment on total sleep, and mGlu receptor selectivity data (PDF)
>
> Molecule SMILES strings and bioactivity (XLSX)

AUTHOR INFORMATION

Corresponding Authors
*A.P.IJ.: phone, +31 (0)71 527 4651; e-mail, ijzerman@lacdr.leidenuniv.nl.
*G.T.: phone, +34 925 24 5777; e-mail, gtresade@its.jnj.com.

ORCID
Andrés A. Trabanco: 0000-0002-4225-758X
Adriaan P. IJzerman: 0000-0002-1182-2259
Gary Tresadern: 0000-0002-4801-1644

Author Contributions
The manuscript was written through contributions of all authors. All authors have given approval to the final version of the manuscript.

Notes
The authors declare no competing financial interest.

ABBREVIATIONS USED

AUC, area under the curve; BCA, bicinchoninic acid; CHO, Chinese hamster ovary; DMEM, Dulbecco's modified Eagle medium; DMSO, dimethyl sulfoxide; GPCR, G-protein-coupled receptor; [^{35}S]GTPγS, guanosine 5′-O-[γ-thio]triphosphate; mGlu, metabotropic glutamate; PAM, positive allosteric modulator; PBS, phosphate buffered saline; RT, residence time; SEM, standard error of the mean; SPA, scintillation proximity assay; VFT, Venus flytrap domain; 7TM, seven transmembrane domain

REFERENCES

(1) Kew, J. N. C.; Kemp, J. A. Ionotropic and Metabotropic Glutamate Receptor Structure and Pharmacology. *Psychopharmacology (Berl).* **2005**, *179*, 4−29.

(2) Niswender, C. M.; Conn, P. J. Metabotropic Glutamate Receptors: Physiology, Pharmacology, and Disease. *Annu. Rev. Pharmacol. Toxicol.* **2010**, *50*, 295−322.

(3) Muto, T.; Tsuchiya, D.; Morikawa, K.; Jingami, H. Structures of the Extracellular Regions of the Group II/III Metabotropic Glutamate Receptors. *Proc. Natl. Acad. Sci. U. S. A.* **2007**, *104*, 3759−3764.

(4) Nicoletti, F.; Bockaert, J.; Collingridge, G. L.; Conn, P. J.; Ferraguti, F.; Schoepp, D. D.; Wroblewski, J. T.; Pin, J. P. Metabotropic Glutamate Receptors: From the Workbench to the Bedside. *Neuropharmacology* **2011**, *60*, 1017−1041.

(5) Dunayevich, E.; Erickson, J.; Levine, L.; Landbloom, R.; Schoepp, D. D.; Tollefson, G. D. Efficacy and Tolerability of an mGlu2/3 Agonist in the Treatment of Generalized Anxiety Disorder. *Neuropsychopharmacology* **2008**, *33*, 1603−1610.

(6) Patil, S. T.; Zhang, L.; Martenyi, F.; Lowe, S. L.; Jackson, K. A.; Andreev, B. V.; Avedisova, A. S.; Bardenstein, L. M.; Gurovich, I. Y.; Morozova, M. A.; Mosolov, S. N.; Neznanov, N. G.; Reznik, A. M.; Smulevich, A. B.; Tochilov, V. A.; Johnson, B. G.; Monn, J. A.; Schoepp, D. D. Activation of mGlu2/3 Receptors as a New Approach to Treat Schizophrenia: A Randomized Phase 2 Clinical Trial. *Nat. Med.* **2007**, *13*, 1102−1107.

(7) Keov, P.; Sexton, P. M.; Christopoulos, A. Allosteric Modulation of G Protein-Coupled Receptors: A Pharmacological Perspective. *Neuropharmacology* **2011**, *60*, 24−35.

(8) Trabanco, A. A.; Cid, J. M. mGluR2 Positive Allosteric Modulators: A Patent Review (2009 - Present). *Expert Opin. Ther. Pat.* **2013**, *23*, 629−647.

(9) Johnson, M. P.; Baez, M.; Jagdmann, G. E.; Britton, T. C.; Large, T. H.; Callagaro, D. O.; Tizzano, J. P.; Monn, J. A.; Schoepp, D. D. Discovery of Allosteric Potentiators for the Metabotropic Glutamate 2 Receptor: Synthesis and Subtype Selectivity of N-(4-(2-Methoxyphenoxy)phenyl)-N-(2,2,2- Trifluoroethylsulfonyl)pyrid-3-Yl-methylamine. *J. Med. Chem.* **2003**, *46*, 3189−3192.

(10) Galici, R.; Jones, C. K.; Hemstapat, K.; Nong, Y.; Echemendia, N. G.; Williams, L. C.; de Paulis, T.; Conn, P. J. Biphenyl-Indanone A, a Positive Allosteric Modulator of the Metabotropic Glutamate Receptor Subtype 2, Has Antipsychotic- and Anxiolytic-like Effects in Mice. *J. Pharmacol. Exp. Ther.* **2006**, *318*, 173−185.

(11) Fell, M. J.; Witkin, J. M.; Falcone, J. F.; Katner, J. S.; Perry, K. W.; Hart, J.; Rorick-Kehn, L.; Overshiner, C. D.; Rasmussen, K.; Chaney, S. F.; Benvenga, M. J.; Li, X.; Marlow, D. L.; Thompson, L. K.; Luecke, S. K.; Wafford, K. A.; Seidel, W. F.; Edgar, D. M.; Quets, A. T.; Felder, C. C.; Wang, X.; Heinz, B. A.; Nikolayev, A.; Kuo, M.; Mayhugh, D.; Khilevich, A.; Zhang, D.; Ebert, P. J.; Eckstein, J. A.; Ackermann, B. L.; Swanson, S. P.; Catlow, J. T.; Dean, R. A.; Jackson, K.; Tauscher-Wisniewski, S.; Marek, G. J.; Schkeryantz, J. M.; Svensson, K. A. N-(4-((2-(Trifluoromethyl)-3-Hydroxy-4-(Isobutyryl)phenoxy)methyl)-benzyl)-1-Methyl-1H-Imidazole-4-Carboxamide (THIIC), a Novel Metabotropic Glutamate 2 Potentiator with Potential Anxiolytic/antidepressant Properties: In Vivo Profiling Suggests a Link between Behavioral and Central Nervous System Neurochemical Changes. *J. Pharmacol. Exp. Ther.* **2011**, 336, 165−177.

(12) Lavreysen, H.; Langlois, X.; Ahnaou, A.; Drinkenburg, W.; te Riele, P.; Biesmans, I.; Van der Linden, I.; Peeters, L.; Megens, A.; Wintmolders, C.; Cid, J. M.; Trabanco, A. A.; Andrés, J. I.; Dautzenberg, F. M.; Lütjens, R.; Macdonald, G.; Atack, J. R. Pharmacological Characterization of JNJ-40068782, a New Potent, Selective, and Systemically Active Positive Allosteric Modulator of the mGlu2 Receptor and Its Radioligand [3H]JNJ-40068782. *J. Pharmacol. Exp. Ther.* **2013**, 346, 514−527.

(13) Cook, D.; Brown, D.; Alexander, R.; March, R.; Morgan, P.; Satterthwaite, G.; Pangalos, M. N. Lessons Learned from the Fate of AstraZeneca's Drug Pipeline: A Five-Dimensional Framework. *Nat. Rev. Drug Discovery* **2014**, 13, 419−431.

(14) Homepage: http://clinicaltrials.gov. The Effects AZD8529 on Cognition and Negative Symptoms in Schizophrenics: https://clinicaltrials.gov/show/NCT00986531 (accessed December 22, 2016).

(15) Homepage: http://clinicaltrials.gov. The Study of AZD8529 for Smoking Cessation in Female Smokers: https://www.clinicaltrials.gov/ct2/show/NCT02401022?term=AZD8529&rank=1 (accessed April 3, 2017).

(16) Cid, J. M.; Tresadern, G.; Duvey, G.; Lütjens, R.; Finn, T.; Rocher, J.; Poli, S.; Vega, J. A.; de Lucas, A. I.; Matesanz, E.; Linares, M. L.; Andrés, J. I.; Alcazar, J.; Alonso, J. M.; Macdonald, G. J.; Oehlrich, D.; Lavreysen, H.; Ahnaou, A.; Drinkenburg, W.; Mackie, C.; Pype, S.; Gallacher, D.; Trabanco, A. A. Discovery of 1-Butyl-3-Chloro-4-(4-Phenyl-1-Piperidinyl)-(1H)-Pyridone (JNJ-40411813): A Novel Positive Allosteric Modulator of the Metabotropic Glutamate 2 Receptor. *J. Med. Chem.* **2014**, 57, 6495−6512.

(17) Lavreysen, H.; Ahnaou, A.; Drinkenburg, W.; Langlois, X.; Mackie, C.; Pype, S.; Lütjens, R.; Le Poul, E.; Trabanco, A. A.; Cid Nuñez, J. M. Pharmacological and Pharmacokinetic Properties of JNJ-40411813, a Positive Allosteric Modulator of the mGlu2 Receptor. *Pharmacol. Res. Perspect.* **2015**, 3, e00096.

(18) Lavreysen, H.; Langlois, X.; Ver Donck, L.; Cid Nuñez, J. M.; Pype, S.; Lütjens, R.; Megens, A. Preclinical Evaluation of the Antipsychotic Potential of the mGlu2-Positive Allosteric Modulator JNJ-40411813. *Pharmacol. Res. Perspect.* **2015**, 3, e00097.

(19) Salih, H.; Anghelescu, I.; Kezic, I.; Sinha, V.; Hoeben, E.; Van Nueten, L.; De Smedt, H.; De Boer, P. Pharmacokinetic and Pharmacodynamic Characterisation of JNJ-40411813, a Positive Allosteric Modulator of mGluR2, in Two Randomised, Double-Blind Phase-I Studies. *J. Psychopharmacol.* **2015**, 29, 414−425.

(20) Kent, J. M.; Daly, E.; Kezic, I.; Lane, R.; Lim, P.; De Smedt, H.; De Boer, P.; Van Nueten, L.; Drevets, W. C.; Ceusters, M. Efficacy and Safety of an Adjunctive mGlu2 Receptor Positive Allosteric Modulator to a SSRI/SNRI in Anxious Depression. *Prog. Neuro-Psychopharmacol. Biol. Psychiatry* **2016**, 67, 66−73.

(21) http://www.addextherapeutics.com/investors/press-releases/news-details/article/addex-reports-top-linedata-from-a-successful-phase-2a-clinical-study-with-adx71149-inschizophrenia/ (accessed July 28, 2016).

(22) A Study of JNJ-40411813 as Supplementary Treatment to an Antidepressant in Adults With Depression and Anxiety Symptoms. http://clinicaltrials.gov/show/NCT01582815 (accessed July 28, 2016).

(23) Swinney, D. C. The Role of Binding Kinetics in Therapeutically Useful Drug Action. *Curr. Opin. Drug Discovery Dev.* **2009**, 12, 31−39.

(24) Copeland, R. A. The Drug−Target Residence Time Model: A 10-Year Retrospective. *Nat. Rev. Drug Discovery* **2016**, 15, 87−95.

(25) Guo, D.; Heitman, L. H.; IJzerman, A. P. The Role of Target Binding Kinetics in Drug Discovery. *ChemMedChem* **2015**, 10, 1793−1796.

(26) Swinney, D. C.; Haubrich, B. A.; Van Liefde, I.; Vauquelin, G. The Role of Binding Kinetics in GPCR Drug Discovery. *Curr. Top. Med. Chem.* **2015**, 15, 2504−2522.

(27) Guo, D.; Heitman, L. H.; IJzerman, A. P. Kinetic Aspects of the Interaction between Ligand and G Protein-Coupled Receptor: The Case of the Adenosine Receptors. *Chem. Rev.* **2017**, 117, 38−66.

(28) Guo, D.; Hillger, J. M.; IJzerman, A. P.; Heitman, L. H. Drug-Target Residence Time-a Case for G Protein-Coupled Receptors. *Med. Res. Rev.* **2014**, 34, 856−892.

(29) Dowling, M. R.; Charlton, S. J. Quantifying the Association and Dissociation Rates of Unlabelled Antagonists at the Muscarinic M3 Receptor. *Br. J. Pharmacol.* **2006**, 148, 927−937.

(30) Tresadern, G.; Bartolome, J. M.; Macdonald, G. J.; Langlois, X. Molecular Properties Affecting Fast Dissociation from the D2 Receptor. *Bioorg. Med. Chem.* **2011**, 19, 2231−2241.

(31) Kapur, S.; Seeman, P. Does Fast Dissociation From the Dopamine D2 Receptor Explain the Action of Atypical Antipsychotics?: A New Hypothesis. *Am. J. Psychiatry* **2001**, 158, 360−369.

(32) Yin, N.; Pei, J.; Lai, L. A Comprehensive Analysis of the Influence of Drug Binding Kinetics on Drug Action at Molecular and Systems Levels. *Mol. BioSyst.* **2013**, 9, 1381−1389.

(33) Vauquelin, G. Effects of Target Binding Kinetics on in Vivo Drug Efficacy: K off, K on and Rebinding. *Br. J. Pharmacol.* **2016**, 173, 2319−2334.

(34) Schoop, A.; Dey, F. On-Rate Based Optimization of Structure−kinetic Relationship − Surfing the Kinetic Map. *Drug Discovery Today: Technol.* **2015**, 17, 9−15.

(35) Cid, J. M.; Tresadern, G.; Vega, J. A.; de Lucas, A. I.; Matesanz, E.; Iturrino, L.; Linares, M. L.; Garcia, A.; Andrés, J. I.; Macdonald, G. J.; Oehlrich, D.; Lavreysen, H.; Megens, A.; Ahnaou, A.; Drinkenburg, W.; Mackie, C.; Pype, S.; Gallacher, D.; Trabanco, A. A. Discovery of 3-Cyclopropylmethyl-7-(4-Phenylpiperidin-1-Yl)-8-trifluoromethyl-[1,2,4]triazolo[4,3-a]pyridine (JNJ-42153605): A Positive Allosteric Modulator of the Metabotropic Glutamate 2 Receptor. *J. Med. Chem.* **2012**, 55, 8770−8789.

(36) Tresadern, G.; Cid, J.-M. M.; Trabanco, A. A. QSAR Design of Triazolopyridine mGlu2 Receptor Positive Allosteric Modulators. *J. Mol. Graphics Modell.* **2014**, 53, 82−91.

(37) Cid-Nunez, J. M.; De Lucas Olivares, A. I.; Trabanco-Suarez, A. A.; MacDonald, G. J. 7-Aryl-1,2,4-triazolo[4,3-A]pyridine Derivatives and Their Use as Positive Allosteric Modulators of mGluR2 Receptors. WO2010130423 A1, 2010.

(38) Cid, J. M.; Duvey, G.; Tresadern, G.; Nhem, V.; Furnari, R.; Cluzeau, P.; Vega, J. A.; de Lucas, A. I.; Matesanz, E.; Alonso, J. M.; Linares, M. L.; Andrés, J. I.; Poli, S. M.; Lutjens, R.; Himogai, H.; Rocher, J.; Macdonald, G. J.; Oehlrich, D.; Lavreysen, H.; Ahnaou, A.; Drinkenburg, W.; Mackie, C.; Trabanco, A. A. Discovery of 1,4-Disubstituted 3-Cyano-2-Pyridones: A New Class of Positive Allosteric Modulators of the Metabotropic Glutamate 2 Receptor. *J. Med. Chem.* **2012**, 55, 2388−2405.

(39) Doornbos, M. L. J.; Pérez-Benito, L.; Tresadern, G.; Mulder-Krieger, T.; Biesmans, I.; Trabanco, A. A.; Cid, J. M.; Lavreysen, H.; IJzerman, A. P.; Heitman, L. H. Molecular Mechanism of Positive Allosteric Modulation of the Metabotropic Glutamate Receptor 2 by JNJ-46281222. *Br. J. Pharmacol.* **2016**, 173, 588−600.

(40) Motulsky, H. J.; Mahan, L. C. The Kinetics of Competitive Radioligand Binding Predicted Mass Action by the Law of Mass Action. *Mol. Pharmacol.* **1984**, 25, 1−9.

(41) Xia, L.; de Vries, H.; IJzerman, A. P.; Heitman, L. H. Scintillation Proximity Assay (SPA) as a New Approach to Determine a Ligand's Kinetic Profile. A Case in Point for the Adenosine A1 Receptor. *Purinergic Signalling* **2016**, 12, 115−126.

(42) Farinha, A.; Lavreysen, H.; Peeters, L.; Russo, B.; Masure, S.; Trabanco, A. A.; Cid, J.; Tresadern, G. Molecular Determinants of

Positive Allosteric Modulation of the Human Metabotropic Glutamate Receptor 2. *Br. J. Pharmacol.* **2015**, *172*, 2383−2396.

(43) Pérez-Benito, L.; Doornbos, M. L. J.; Cordomí, A.; Peeters, L.; Lavreysen, H.; Pardo, L.; Tresadern, G. Molecular Switches of Allosteric Modulation of the Metabotropic Glutamate 2 Receptor. *Structure* **2017**, *25*, 1153−1162.

(44) Lovering, F.; Bikker, J.; Humblet, C. Escape from Flatland: Increasing Saturation as an Approach to Improving Clinical Success. *J. Med. Chem.* **2009**, *52*, 6752−6756.

(45) Wacker, D.; Wang, S.; McCorvy, J. D.; Betz, R. M.; Venkatakrishnan, A. J.; Levit, A.; Lansu, K.; Schools, Z. L.; Che, T.; Nichols, D. E.; Shoichet, B. K.; Dror, R. O.; Roth, B. L. Crystal Structure of an LSD-Bound Human Serotonin Receptor. *Cell* **2017**, *168*, 377−389.

(46) Sykes, D. A.; Dowling, M. R.; Charlton, S. J. Exploring the Mechanism of Agonist Efficacy: A Relationship between Efficacy and Agonist Dissociation Rate at the Muscarinic M3 Receptor. *Mol. Pharmacol.* **2009**, *76*, 543−551.

(47) Guo, D.; Mulder-Krieger, T.; IJzerman, A. P.; Heitman, L. H. Functional Efficacy of Adenosine A2A Receptor Agonists Is Positively Correlated to Their Receptor Residence Time. *Br. J. Pharmacol.* **2012**, *166*, 1846−1859.

(48) Deyrup, M. D.; Nowicki, S. T.; Richards, N. G.; Otero, D. H.; Harrison, J. K.; Baker, S. P. Structure-Affinity Profile of 8-Hydroxycarbostyril-Based Agonists That Dissociate Slowly from the beta2-Adrenoceptor. *Naunyn-Schmiedeberg's Arch. Pharmacol.* **1999**, *359*, 168−177.

(49) Mould, R.; Brown, J.; Marshall, F. H.; Langmead, C. J. Binding Kinetics Differentiates Functional Antagonism of Orexin-2 Receptor Ligands. *Br. J. Pharmacol.* **2014**, *171*, 351−363.

(50) Sykes, D. a; Charlton, S. J. Slow Receptor Dissociation Is Not a Key Factor in the Duration of Action of Inhaled Long-Acting β2-Adrenoceptor Agonists. *Br. J. Pharmacol.* **2012**, *165*, 2672−2683.

(51) Yu, Z.; Van Veldhoven, J. P. D.; Louvel, J.; 'T Hart, I. M. E.; Rook, M. B.; Van Der Heyden, M. A. G.; Heitman, L. H.; IJzerman, A. P. Structure-Affinity Relationships (SARs) and Structure-Kinetics Relationships (SKRs) of Kv11.1 Blockers. *J. Med. Chem.* **2015**, *58*, 5916−5929.

(52) Yu, Z.; IJzerman, A. P.; Heitman, L. H. K v 11.1 (hERG)-Induced Cardiotoxicity: A Molecular Insight from a Binding Kinetics Study of Prototypical K v 11.1 (hERG) Inhibitors. *Br. J. Pharmacol.* **2015**, *172*, 940−955.

(53) de Witte, W. E. A.; Danhof, M.; van der Graaf, P. H.; de Lange, E. C. M. In Vivo Target Residence Time and Kinetic Selectivity: The Association Rate Constant as Determinant. *Trends Pharmacol. Sci.* **2016**, *37*, 831−842.

(54) Vauquelin, G.; Charlton, S. J. Long-Lasting Target Binding and Rebinding as Mechanisms to Prolong in Vivo Drug Action. *Br. J. Pharmacol.* **2010**, *161*, 488−508.

(55) Vauquelin, G. On the "micro"-Pharmacodynamic and Pharmacokinetic Mechanisms That Contribute to Long-Lasting Drug Action. *Expert Opin. Drug Discovery* **2015**, *10*, 1085−1098.

(56) Vauquelin, G. Cell Membranes...and How Long Drugs May Exert Beneficial Pharmacological Activity in Vivo. *Br. J. Clin. Pharmacol.* **2016**, *82*, 673−682.

(57) Perry, D. C.; Mullis, K. B.; Øie, S.; Sadée, W. Opiate Antagonist Receptor Binding in Vivo: Evidence for a New Receptor Binding Model. *Brain Res.* **1980**, *199*, 49−61.

(58) Yu, N.; Atienza, J. M.; Bernard, J.; Blanc, S.; Zhu, J.; Wang, X.; Xu, X.; Abassi, Y. Real-Time Monitoring of Morphological Changes in Living Cells by Electronic Cell Sensors Arrays: An Approach to Study G Protein-Coupled Receptors. *Anal. Chem.* **2006**, *78*, 35−43.

(59) Hillger, J. M.; Diehl, C.; van Spronsen, E.; Boomsma, D. I.; Slagboom, P. E.; Heitman, L. H.; IJzerman, A. P. Getting Personal: Endogenous Adenosine Receptor Signaling in Lymphoblastoid Cell Lines. *Biochem. Pharmacol.* **2016**, *115*, 114−122.

(60) Xi, B.; Yu, N.; Wang, X.; Xu, X.; Abassi, Y. A. The Application of Cell-Based Label-Free Technology in Drug Discovery. *Biotechnol. J.* **2008**, *3*, 484−495.

(61) Ahnaou, A.; Dautzenberg, F. M.; Geys, H.; Imogai, H.; Gibelin, A.; Moechars, D.; Steckler, T.; Drinkenburg, W. H. I. M. Modulation of Group II Metabotropic Glutamate Receptor (mGlu2) Elicits Common Changes in Rat and Mice Sleep-Wake Architecture. *Eur. J. Pharmacol.* **2009**, *603*, 62−72.

(62) Ahnaou, A.; De Boer, P.; Lavreysen, H.; Huysmans, H.; Sinha, V.; Raeymaekers, L.; Van De Casteele, T.; Cid, J. M.; Van Nueten, L.; MacDonald, G. J.; Kemp, J. A.; Drinkenburg, W. H. I. M. Translational Neurophysiological Markers for Activity of the Metabotropic Glutamate Receptor (mGluR2) Modulator JNJ-40411813: Sleep EEG Correlates in Rodents and Healthy Men. *Neuropharmacology* **2016**, *103*, 290−305.

(63) Cuisset, L.; Tichonicky, L.; Jaffray, P.; Delpech, M. The Effects of Sodium Butyrate on Transcription Are Mediated through Activation of a Protein Phosphatase. *J. Biol. Chem.* **1997**, *272*, 24148−24153.

(64) Hillger, J. M.; Schoop, J.; Boomsma, D. I.; Eline Slagboom, P.; IJzerman, A. P.; Heitman, L. H. Whole-Cell Biosensor for Label-Free Detection of GPCR-Mediated Drug Responses in Personal Cell Lines. *Biosens. Bioelectron.* **2015**, *74*, 233−242.

(65) Cheng, Y.-C.; Prusoff, W. H. Relationship between the Inhibition Constant (KI) and the Concentration of Inhibitor Which Causes 50 per Cent Inhibition (I50) of an Enzymatic Reaction. *Biochem. Pharmacol.* **1973**, *22*, 3099−3108.